ASHESI UNIVERSITY COLLEGE

A REUSABLE, LOW-COST AND SELF-SUFFICIENT SENSOR-BASED NEONATAL PULSE OXIMETER

CAPSTONE PROJECT

B.Sc. Electrical and Electronics Engineering

Rosemond Nyatefe Tawiah

2022

ASHESI UNIVERSITY COLLEGE

A Reusable, Low-Cost and Self-Sufficient Sensor-Based Neonatal Pulse Oximeter

CAPSTONE PROJECT

Capstone Project submitted to the Department of Engineering, Ashesi University College in partial fulfilment of the requirements for the award of Bachelor of Science degree in Electrical and Electronics Engineering.

Rosemond Nyatefe Tawiah

2022

DECLARATION

I hereby declare that this capstone is the result of my own original work and that no part of it has been presented for another degree in this university or elsewhere.

Candidate's Signature:

……

Candidate's Name:

……

Date:

……

I hereby declare that preparation and presentation of this capstone were supervised in accordance with the guidelines on supervision of capstone laid down by Ashesi University College.

Supervisor's Signature:

……

Supervisor's Name:

……

Date:

……

Acknowledgements

I want to first thank the Almighty God for the strength and knowledge to complete this project. I would like to thank my supervisor, Dr Elena Rosca for her unwavering support, guidance and encouragement through the period of working on this project. To all the people whose encouragement and academic advice helped me undertake this project including Dr Nathan Amankwah, and Kofi Adu-Labi, I am very grateful. To, my family and my very good friends, God bless you for being a stronghold of support.

Abstract

Pulse oximeters are non-invasive medical health devices for measuring oxygen saturation and pulse rate of humans. Pulse oximeters used for neonates have been identified to have some limitations in terms of their bulkiness in size, the need for a pulse sensor attachment to a monitoring device to obtain readings and their expensive nature. This project explores a pulse oximeter design to eliminate these limitations and create an accurate alternative for neonatal pulse oximeters. The proposed design includes a pulse sensor and a control and display circuit self-sufficiently powered by a direct current source of voltage. It employs analog signal processing, digital signal processing (DSP) with a low-power but highly efficient microprocessor to ensure accurate values are obtained. The project explores this design but however implemented part of the design (Infrared (IR) sensor) based on the materials and electrical components available. Even though the proposed design was not built as whole, various sections of the design was implemented or simulated and were feasible. The results from the IR sensor built was compared to a commercial pulse oximeter and from the statistical analysis conducted, the two systems have similar readings confirmed by the t-value of 0.917 in the paired t-test. Unfiltered data was used with the algorithm developed and the DSP and the readings for the SpO_2 and pulse rate were similar to the commercial oximeter.

Table of Content

DECLARATION i

Acknowledgements ii

Abstract iii

List of Tables vi

List of Figures vii

Chapter 1: Introduction 1

1.1 Background 1
1.3 Problem Definition 3
1.4 Proposed Solution 4
Chapter 2: Literature Review 5

2.1 Introduction to Pulse Oximetry 5
2.1.1 Pulse Oximetry Theory 6

2.1.2 Photoplethysmography 9

2.1.3 Beer's Law in Pulse Oximetry 10

2.2 Development of Pulse Oximeters 15
2.2.1 History –Introduction to pulse oximetry 15

2.2.2 Existing Pulse Oximetry Innovations 16

2.2.3 Review and Limitations in existing solutions 17

2.3 Analogue and Digital Pulse Oximeter Design Approach 18
Chapter 3: Design 20

3.1 User Requirements 20
3.2 Design Requirements 20
3.2.1 Hardware requirements 20

3.2.2 Software requirements 21

Chapter 4: Methodology 23

4.1 Block Diagram 23
4.2 Hardware Design 25
4.2.1 Electrical Design 25
4.2.2 Mechanical Design 31
4.3 Software Design 32
4.3.1 System Clock, Crystal and MCU Code Upload 32
4.3.2 Timers and Pulse Width Modulation (PWM) 32
4.3.3 Interrupts 33
4.3.4 Analogue-to-Digital Conversion (ADC) 33
4.3.5 I2C Organic Light Emitting Diode (OLED) 33
4.3.6 Program Flow Chart 34
4.4 Design of Digital Signal Processing using MK64FN1M0VLL12 34
4.5 SpO_2 and Pulse Rate Calculations (BPM) 36
4.6 Updated Prototype Design 37
Chapter 5: Testing, Results and Discussion 41
5.1 Power Circuit 41
5.2 Pulse Sensor Circuit 41
5.3 Analog Signal Processing Circuit 43
5.4 Digital Signal Processing 46
5.5 Pulse Oximeter Readings 52
5.6 Statistical Analysis 54
5.7 Cost Analysis 56
Chapter 6: Conclusion 57
6.2 Future work 58
References 59
Appendix 64

List of Tables

Table 4.1: Some operating features of MK64FN1M0VLL12 and STM32F446……30

Table 4.2: Pugh chart for MCU selection…….. 31

Table 4.3: FIR band pass filtering parameter specifications…… 35

Table 5.1: Recorded current outputs for the detection of RED and IR signals by OP999… 42

Table 5.2: Summarized pulse rate and SpO_2 readings obtained using Physionet dataset…. 52

Table 5.3: Pulse readings from IR Sensor built and the Lk87 Pulse oximeter…….. 53

Table 5.4: Results from the two-sided paired T-test…….. 55

Table 5.5: Cost breakdown of building the proposed neonatal pulse oximeter design…… 56

List of Figures

Figure 2.1: Transmission and reflectance mode of pulse oximetry……..7

Figure 2.2: The calibration curves for a pulse……..8

Figure 2.3: Photoplethysmography signal acquired from a living tissue……...10

Figure 2.4: A PPG waveform with its AC and DC……10

Figure: 2.5 Extinction coefficient of deoxygenated haemoglobin (Hb) and oxygenated haemoglobin (HbO_2)…….13

Figure 2.6 Beer's law in pulse oximetry…….14

Figure 4.1: Image of the system's block diagram……..24

Figure 4.2: Image of the power circuitry……...26

Figure 4.3: Image of the (a) LED Drive Circuitry (b) Pulse sensor circuit…….26

Figure 4.4: Image of the Analog Signal Conditioning Circuitry……28

Figure 4.5: Image of the control circuitry……..29

Figure 4.6: Image of program flow chart of system software……34

Figure 4.7 Image of the LED Drive Circuitry……38

Figure 4.8: Image of the Transimpedance Amplifier Circuit…….39

Figure 4.9 Image of the Voltage Regulating Circuit for 3.3V Supply……40

Figure 5.1: Image of power circuit simulation in the proteus software……..41

Figure 5.2: Timing diagram for the alternate switching of the RED (green) and IR (blue) LEDs…….42

Figure 5.3: DC voltage plot for the output of the transimpedance amplifier…….43

Figure 5.4: Bode plot of implemented passive low pass filter……..44

Figure 5.5: Bode plot of implemented passive high pass filter……..45

Figure 5.6: Plot showing output of gain amplifying circuit……..46

Figure 5.7: Bode plot of FIR bandpass designed……...47

Figure 5.8: Time and Frequency domain plots of FIR filter outputs…….47

Figure 5.9: Plots showing the effect of FIR bandpass filtering on IR signals of Physionet dataset……...49

Figure 5.10: Plots showing unfiltered IR signals of Physionet dataset……..49

Figure 5.11: Plots showing filtered IR signals of Physionet dataset……..50

Figure 5.12: Plots showing the effect of FIR bandpass filtering on RED signals of Physionet dataset……...50

Figure 5.13: Plots showing unfiltered RED signals of Physionet dataset…….51

Figure 5.14: Plots showing filtered RED signals of Physionet dataset……..51

Figure 5.15: Plots showing the effect of FIR bandpass filtering on IR signals of the IR Sensor built……...52

Figure 5.16: Pulse Readings for IR Sensor built…….54

Figure 5.17: Pulse Readings Lk87 pulse Oximeter…….54

Figure 5.18: Graph showing similarity between IR sensor built and the Lk87 fingertip pulse Oximeter……...56

Chapter 1: Introduction

1.1 Background

Pulse oximetry has become a major breakthrough in medicine and its practice specifically due to its accurate and non-invasive approach to monitor oxygenation levels in humans [1]. Pulse Oximetry uses Photoplethysmography (PPG) which is an optical, low-cost method to obtain pulsatile signals which indicate the change in volume of blood in the tissue [2]. PPG signals are acquired through non-invasive methods to take measurements on the surface of the skin. Pulse oximeters are thus, non-invasive health devices used to monitor the health of people who suffer from any type of condition which affects their blood oxygen levels including Chronic Obstructive Pulmonary Disease (COPD), Asthma, Cardiovascular conditions, and Pneumonia [3]. This device is mainly used for measuring pulse rate and the saturation of haemoglobin in arterial blood [4]. Oxygen blood level and the flow of blood (blood velocity) are parameters that could help in the detection of congenital heart disease (CHD) and other heart, or blood related not only in infants but adults as well [5]. For adults, pulse oximeters are placed on the fingers, earlobes or foreheads while infants have pulse oximeters placed around the foot or the toe or the ear lobe.

Congenital heart diseases or defects are one of the most common birth defects that occur when the heart or blood vessels near the heart do not develop normally before birth [6]. Globally, approximately one percent of live births (approximately 5 to 15 out of 1,000 live births) are affected by CHD and would require surgical interventions to improve the quality of life [7], [8]. In developing countries like Ghana, research [7] showed that CHDs are either diagnosed late or not diagnosed entirely, contributing to a significant fraction of child mortality and morbidity. In this regard, mortality and morbidity rates of children could be reduced by approximately thirty percent if birth defects such as CHD are detected earlier [5].

Recent research and developments in pulse oximetry presents evidence that the use of pulse oximeters coupled with neonatal physical examinations provides an optimal and moderately sensitive test for the detection of CHD with a very low rate of false-positive (0.14 %) [9], [10]. Using both pulse oximetry and physical examinations had sensitivity of 0.92 (CI 95%, 0.87-0.95), and specificity: 0.98 (CI 95%, 0.89-1.00) as compared to only physical examinations with sensitivity of 0.53 (CI 95%, 0.28-0.78) and specificity: 0.99 (CI 95%, 0.97-1.00) The research in [9] also suggests that this method is essential in low and middle-income settings like rural areas where there is a lack in technological medical support. Thus, the use of pulse oximetry in rural areas and even urban locations in developing countries like Ghana could aid in the early detection of CHDs in neonates if low-cost pulse oximeters are supplied to all medical units across the country and compulsory screening is instituted before neonates are discharged after birth.

Pulse oximeters have become a revolutionary invention in the health sector but have also had their own setbacks especially with neonatal pulse oximeters. The type of pulse oximeters used for older infants are usually the lightweight-bulky ones. For younger infants or neonates especially in the Intensive Care Units (ICUs), the sensor-based pulse oximeters such as the Nonin 6000ci Infant Cloth Disposable Sensors are used [11]. These sensor-based pulse oximeters used in the ICU are still bulky in nature with a lot of wires restricting movement of the neonate and their comfort. They are also not self-sufficient (in terms of power supply and display) and require to be connected to a central monitoring device where readings are recorded. In addition, sensors like the Nonin 6000ci Infant Cloth Disposable Sensors are non-reusable and would have to be replaced periodically. In the context of the Ghanaian health sector for instance, health workers that were contacted during this project confirmed that pulse oximeters are not readily available. Many of the pulse oximeters used in Ghana are used in private hospitals and in the Intensive Care Units (ICU) and triage units

of some public hospitals. Many public health facilities especially in the rural areas and disadvantaged communities lack basic health technologies with the pulse oximeter not being an exception.

1.2 Motivation

The motivation behind this project is to make the pulse oximeter available to most health facilities especially in the rural areas to help in the early detection of birth defects like CHD in new-borns to reduce new-born mortality rate in the country by designing a low-cost solution. Even though the aim is to design more affordable pulse oximeters to help in the early detection of birth defects like CHD, another objective is to ensure comfortability of neonates and efficient readings with this design. With the help of pulse oximeters coupled with other medical examinations, health workers can request further testing for heart related diseases in infants and help prevent future complications, thus improving health care of new-borns and reducing mortality and morbidity rates of infants.

1.3 Problem Definition

Pulse oximeters currently used for neonates are bulky with a lot of wires. They are in addition not self-sufficient and have their sensors connected to a monitoring device which restricts the mobility of the device and that of the neonates as well considering the frequent movement of their arms and legs where pulse sensors are usually attached. This lack of self-sufficiency feature applies to not only the display of the device's readings but also the source of power. On some occasions which are very rare, some pulse sensors have been noted to cause burns to the skin of neonates from a long-term use and direct contact to the skin [12], [13]. Some recently used pulse sensors are made of materials like cloth which cause these sensors to be disposable and used on only one patient beating the sustainability feature of these sensors. In addition to these irregularities with pulse oximeters for neonates, in most

developing countries, the pulse oximeter is available in only few health facilities across the country, with a major lack in rural areas and thus deprives more neonates from getting non-invasively screened for their oxygenation and pulsatile vitals.

1.4 Proposed Solution

This project aims to design and fabricate a Reusable, Low-Cost, and Self-Sufficient (in terms of power supply and display) Sensor-Based Neonatal Pulse Oximeter. The device will use the transmittance approach in the design of the pulse sensor which is regarded a highly accurate approach and mostly used in infant pulse oximeters. The pulse oximeter will have a self-sufficient low power supply (battery) and comprise of the transmittance pulse sensor which is made up of a Red and an InfraRed Light Emitting Diodes (LEDs) for transmission by switching on alternately with a specified duty cycle, and a photodiode for detecting and receiving the transmitted light signals. The output of the pulse sensor will then be connected to the control circuit which consists of a light intensity to current converter, an analogue signal conditioning circuitry with a filter to remove unwanted signals and ambient light noise, an amplifier to amplify very low signals, and a low energy-consumption microprocessor with high-performance data processing algorithms for computation of pulse rate and the saturation of haemoglobin in arterial blood and a display screen to display the measurements.

Chapter 2: Literature Review

Pulse Oximetry's benefits have been significant in modern health care delivery. The science and engineering behind the development of such a device have also improved over the years. There have also been numerous designs and modifications to subsequent inventions in this space. This chapter presents a critical literature review of the pulse oximetry space outlining general pulse oximetry principles, the science and engineering behind such a device, the history and development of non-invasive pulse oximeters, modifications that have been done in this space, recent innovations and developments and, some challenges which pulse oximeters possess.

2.1 Introduction to Pulse Oximetry

Pulse oximetry is a quick non-invasive health method for measuring oxygen blood saturation and pulse rate of an individual. Pulse oximeters are widely used in hospitals during anaesthesiology as a requirement in intensive care units, for emergency purposes and in general health care [14]. It has become another essential vital measured in modern health practice in addition to the more conventional ones, such as body temperature, blood pressure, glucose level, and heart rate. The operation of the pulse oximeter lies at the nexus of the circulatory and respiratory system of a human. These systems are required to work together to deliver oxygen to the cells of the body. The respiratory system has the primary role of taking in oxygen and giving out carbon dioxide. The oxygen taken in is delivered to the cells throughout the body with the circulatory system [15]. A deficiency of oxygen reaching the cells and the tissues of the human body will cause the human body to reach an unstable stage where it metabolizes anaerobically and may cause cells to die if this condition persists [16]. It is therefore important to have devices such as pulse oximeters to detect these irregularities in human systems. A bench-top co-oximeter or blood gas analyser is a device that can be used in the hospital laboratory to assess the oxygen content of the blood.

However, the necessity for immediate clinical information, as well as the need to reduce the time and cost of taking a blood sample and analysing it in the lab, has led to the quest for non-invasive optical technologies such as the pulse oximeter [17]. Pulse oximetry has also been found to be beneficial in diagnosis of certain health defects like congenital heart defects in new-borns which might have been missed during antenatal ultrasound and postnatal examination [16].

2.1.1 Pulse Oximetry Theory

The pulse oximeter is a device which allows for the effective monitoring of blood oxygenation without the need to calibrate the instrument before every use. Oximetry is the measurement of oxygen content in blood and tissues using optical methods. Pulse oximetry is a well-established method for non-invasively monitoring Arterial Oxygen Saturation (SaO_2) in a variety of clinical settings [18]. S_aO_2 refers to the proportion of functional arterial haemoglobin that is oxygenated. The detection of the time-variant photoplethysmography signal that is induced by variations in arterial blood volume allied with cardiac contraction is the basis of pulse oximetry. A functional haemoglobin is able to bind with oxygen while a non-functional haemoglobin cannot bind with oxygen. When functional haemoglobin connects with four oxygen molecules, it is designated oxygenated haemoglobin (HbO_2). It is said to be a deoxygenated or reduced haemoglobin when it carries less than four oxygen molecules (Hb). The measurement of the functional haemoglobin using pulse oximetry assumes that only HbO_2 and Hb are present in the blood. The measurement by the pulse oximeter is therefore known as the Saturation of Peripheral Oxygen (SpO_2) which is an estimation of the concentration of oxygen based on peripheral measurements usually at the earlobe, fingertip or across the toe or foot for neonates. The SpO_2 can be obtained through the formular:

Equation 1

$$SpO_2 = \frac{HbO_2}{Hb+HbO_2} \ ,$$

where HbO_2 = oxygenated haemoglobin and Hb = Deoxygenated or reduced haemoglobin

Pulse oximetry adopts the use of varying light absorption rates in its computations. The rate of light absorption by HbO_2 and Hb differ, and pulse oximetry takes advantage of this characteristic for its computations.

Pulse oximeter sensors are either the transmittance type or the reflectance type. The transmittance type usually has the transmitters (usually Red and Infrared LEDs) directly opposite the receiver which is usually a photodiode (PD) or a photodetector. The reflectance pulse oximeters have the LEDs and the photodiodes adjacent to each other [19], [20].

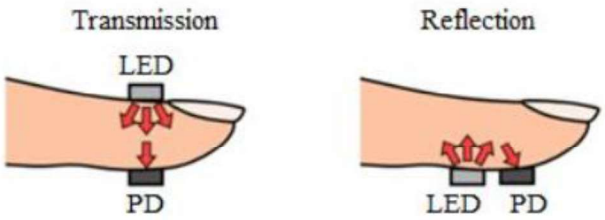

Figure 2.1: Transmission and reflectance mode of pulse oximetry

The LEDs are switched on alternately to capture the transmitted light waves by the single photodiode. A pulse oximeter uses red light (600-750 nm wavelength) and infrared light (850-1000 nm wavelength) absorption characteristics of HbO_2 and Hb to determine the oxygen saturation of human blood. The amount of red or infrared light transmitted is used to obtain an estimate of the ratio between HbO_2 and Hb based on extinction or absorption curves derived from many measurements of a healthy patient at various SpO_2 levels.

The flow of blood is not constant and thus pulses as light is transmitted through it when the pulse oximeter is in use. Since the volume of blood varies because of the pulsations, the rate at which light is absorbed by the bloodless tissue, venous blood, and arterial blood also change. The pulsating nature of the change in volume of blood at a particular time results in the pulsatile (AC) component, synchronous with heartbeats which is approximately one percent of the detected signal. The low-frequency non-pulsatile (DC) part is originated from thermoregulation, respiration, and sympathetic nervous system functions [21] and makes up the greater part of the signal. The detected AC signal is filtered through signal conditioning and is used to find the intermediate ratio value (R) which is then used to find the oxygen saturation based on the empirical data or from the calibration curve.

Equation 2

$$R = \frac{(\frac{ACrms\ 660nm}{DC\ 660nm})}{(\frac{ACrms\ 940nm}{DC\ 940nm})}$$

Below is a graph of a sample calibration curve or eempirical Oxygen Saturation Curve.

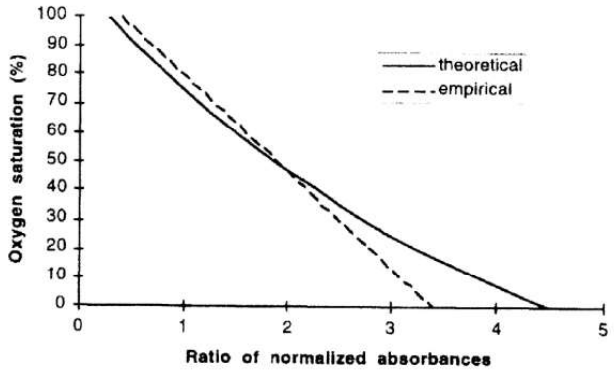

Figure 2.2: The calibration curves for a pulse oximeter [22]

A linearised equation can be obtained from the curve to make the estimation much easier.

Equation 3

$$SpO_2 = 110 - 25\ X\ R$$

Where SpO_2 is the Saturation of Peripheral Oxygen and R is the estimated ratio of of reduced haemoglobin to oxygenated arterial haemoglobin.

2.1.2 Photoplethysmography

Photoplethysmography (PPG) is a simple, low-cost, non-invasive optical technique that can be used to detect the changes in blood volume in the microvascular bed of tissue. Measurements through the adoption of this non-invasive technique are usually taken on the surface of the skin [23]. PPG signals consists of both AC and DC signals. The pulsatile AC signals are generated from the changes in the volume of blood per heartbeat whiles the DC component with various lower frequency components is attributed to respiration, sympathetic nervous system activity and thermoregulation. Even though the source of PPG signals is unknown, they are acknowledged because of their utility in gaining information about the cardiovascular system. [21]. PPG requires a transmitting light source like a Light Emitting Diode (LED) and a receiving component like the photodiode or photodetector that receives the transmitted light wave. Further filtering is done to obtain the wanted frequency signals and the wanted health parameter like oxygen saturation in the blood is obtained.

There are two main PPG operational configurations: Transmission ('trans-illumination') mode operation, in which the tissue sample (e.g., fingertip) is put between the source and detector, and reflection ('adjacent') mode operation, in which the LED and detector are placed side by side. Even though the transmission mode has been noted to provide restrictions in terms of placement, this mode offers more accurate readings [24].

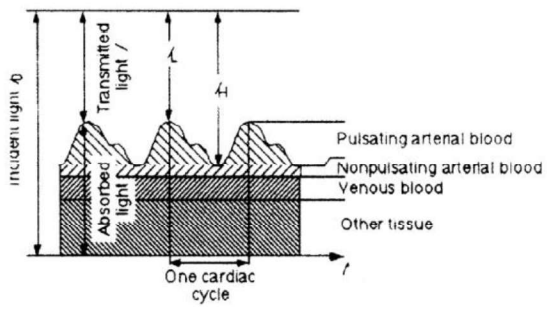

Figure 2.3: Photoplethysmography signal acquired from a living tissue [22]

PPG is applied in many health devices in current modern health care. These include pulse oximeters, blood pressure and cardiac output devices, and even used in assessing autonomic functions and detecting peripheral vascular disease.

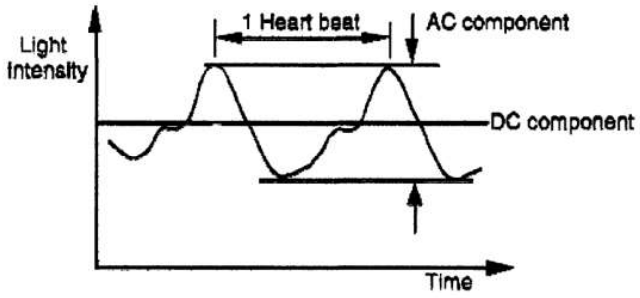

Figure 2.4: A PPG waveform with its AC and DC [22]

2.1.3 Beer's Law in Pulse Oximetry

Pulse oximetry has its operation also based on the principles of the absorption of light. The Beer–Lambert–Bouguer (BBL) law also known as the Beer-Lambert Law, proposed by Pierre Bouguer and Johann Heinrich Lambert gives the simplest assumption that the loss of the intensity of light transmitted through an infinitesimally thin layer of a homogeneous medium is proportional to this intensity and to the layer thickness [25]. In other terms, it refers to the attenuation of monochromatic light passing through a homogeneous medium made up of absorbing material. The law is expressed in the equation:

Equation 4

$I = I_0 e^{-\varepsilon(\lambda)cd}$

where I is the transmitted light, I_0 is the incident light, ε(λ) is the absorptivity or extinction coefficient (usually measured in $Lmmol^{-1}cm^{-1}$) of the material at a particular wavelength, c (usually measured in $mmolL^{-1}$) is a medium specific constant parameter representing the absorbing substance concentration, and d is the optical path length through the matter.

The ratio of the transmitted light to the incident light is called the transmittance of light (T) whose equation we can obtain from the Beer's law as:

Equation 5

$T = (I/I_0)\, e^{-\varepsilon(\lambda)cd}$

and the unscattered absorbance of light defined as the negative natural logarithm of the transmittance of light.

Equation 6

$A = -\ln T = \varepsilon^{(\lambda)cd}$

Applying the superposition property of Beer's law, we can obtain the total absorption A_t of each constituent of a medium since Beer's law makes the principle of substance absorption in medium valid for more than one substance. Thus, using the equation for unscattered absorbance, the total absorbance in a medium can be found as:

Equation 7

$A_t = \sum \varepsilon_i(\lambda)c_i d_i = \varepsilon_1\,(\lambda)c_1 d_1 + \varepsilon_2\,(\lambda)c_2 d_2 + \cdots + \varepsilon_n\,(\lambda)c_n d_n$

where $\varepsilon_i\,(\lambda)$, c_i and d_i are the extinction coefficient, absorbing substance concentration, and optical path length through the matter, respectively.

In humans, haemoglobin is the main element present in human blood which absorbs light at the same wavelengths as used in pulse oximetry. The behaviour expressed by haemoglobin while absorbing light depends on the wavelength of the incident light and its chemical binding. In healthy adults' functional haemoglobin or oxygenated (HbO_2) and reduced haemoglobin (Hb) are the most common type of haemoglobin in the blood. Oxygen saturation is calculated from these types of haemoglobin as:

Equation 8

$$SO_2 = \frac{HbO_2}{Hb + HbO_2} = \frac{CHbO_2}{CHb + CHbO_2}$$

where $CHbO_2$ = concentration of oxygenated haemoglobin and CHb= concentration of deoxygenated haemoglobin

Equation 9

$$CHbO_2 = SO_2 \times (CHb + CHbO_2)$$

Equation 10

$$CHb = (1 - SO_2) \times (CHb + CHbO_2)$$

In pulse oximetry, the most preferred wavelengths are 660 nm for red and 940 for infrared lights. The absorption of light at these wavelengths differs significantly between haemoglobin bonded with oxygen and haemoglobin lacking oxygen. Oxygenated blood absorbs more infrared light whiles allowing more red light to pass through it. This is opposite for deoxygenated blood which allows for more red-light absorption and allowing more infrared light to pass through [26].

One of the main reasons for the pulse oximetry wavelength preference is that light absorption at 660nm fluctuates a lot due to the considerable difference in extinction coefficients between Hb and HbO_2 even with slight variations of oxygen saturation. Another

factor is the availability of LEDs in the above-mentioned wavelengths, which helps to make commercial oximeters more cost-effective.

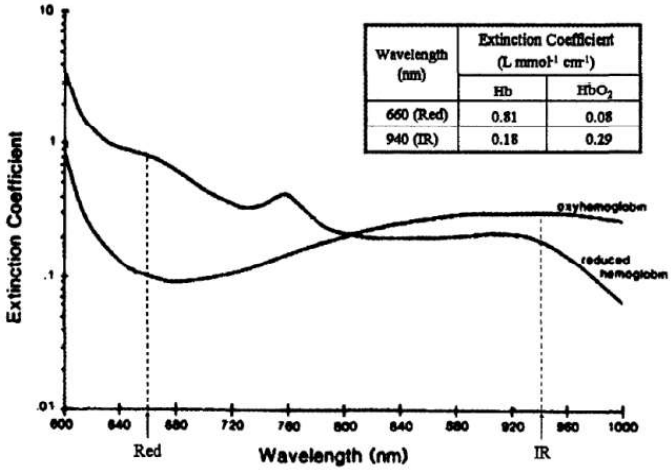

Figure: 2.5 Extinction coefficient of deoxygenated haemoglobin (Hb) and oxygenated haemoglobin (HbO_2) [22]

Considering the optical path length through the matter (d) as the same for Hb and HbO_2, the total light absorption of the blood can be achieved based on Beer's Law and substitutions from equation (9) and (10) as:

$A_t = \varepsilon_{HbO2}(\lambda) c_{HbO2} d_{HbO2} + \varepsilon_{Hb}(\lambda) c_{Hb} d_{Hb}$ now gives,

Equation 11

$$A_t = [\varepsilon_{HbO2}(\lambda) \times SO_2 + \varepsilon_{Hb}(\lambda) \times (1 - SO_2)] (CHb + CHbO_2)\, d$$

Pulse oximeters can benefit from arterial pulsation since light absorption and arterial blood pulsation are inter-related. During systole which occurs during the cardiac cycle, the optical path length in the arteries enlarges as a result of the presence of more haemoglobin which increases light absorption in the tissues with a low peak in transmitted light. This is opposite to diastole where there is high peak in transmitted light due to a reduction in the optical path length in the arteries. The transmitted light's signal which changes in time is

known as the plethysmography (or photoplethysmography) signal. This signal consists of both AC and DC signals. The AC signals are approximately 0.5 to 2 percent of the DC signals. The transmitted signals when at low peak and a high peak can be represented by the equations:

Equation 12

$$I_H = I_0 exp[-\varepsilon_{DC} c_{DC} d_{DC}] \times \exp\left[-(\varepsilon_{HbO} c_{HbO} + \varepsilon_{HbO2}\, c_{HbO2})\, dmin\right]$$

Equation 13

$$I_L = I_0 exp[-\varepsilon_{DC} c_{DC} d_{DC}] \times \exp\left[-(\varepsilon_{HbO} c_{HbO} + \varepsilon_{HbO2}\, c_{HbO2})\, dmax\right]$$

The figure below illustrates the application of beer's law in pulse oximetry.

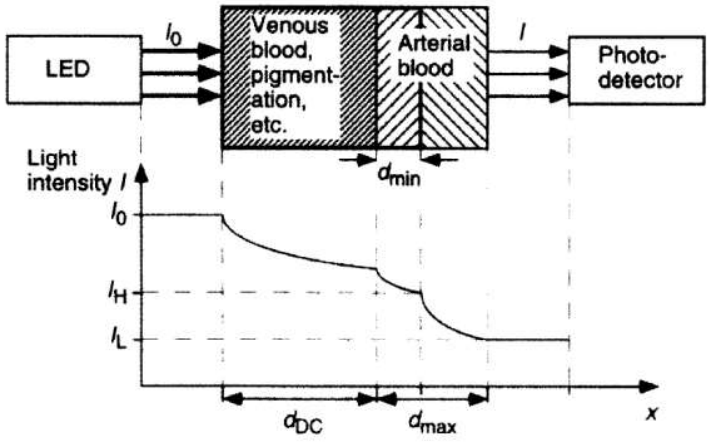

Figure 2.6 Beer's law in pulse oximetry [22]

To be able to compare the light intensities of different wavelengths, we need to first normalize the measured quantities. This is because LEDs emit different intensities of light and may possess a different sensitivity at different wavelengths. By normalizing I_L with respect to I_H, we obtain $\Delta d = dmax - dmin$ which gives the normalized equation:

Equation 14

$$\frac{IL}{IH} = \exp\left[-(\varepsilon_{HbO} c_{HbO} + \varepsilon_{HbO2}\, c_{HbO2})\, \Delta d\right]$$

The natural logarithm of the normalized signal is then calculated to find the total absorbance of the AC component in the light pathway. This gives a new constant light level and the ratio, R, of this normalized absorbance which is represented by the transmitted light during diastole. The red and IR wavelengths are used to calculate the absorbance, which reveals the light absorbers in the arteries.

Equation 15

$$R = \frac{A_{t,R}}{A_{t,IR}} = \frac{-In(\frac{I_{L,R}}{I_{H,R}})}{-In(\frac{I_{L,IR}}{I_{H,IR}})} = \frac{(i_{ac,R} \,/\, i_{dc,R})}{(i_{ac,IR} \,/\, i_{dc,IR})}$$

Where $I_{L,\,R}$, $I_{H,\,R}$, $I_{L,\,IR}$, $I_{H,\,IR}$ denote the low and high intensities of red and infrared wavelengths respectively.

2.2 Development of Pulse Oximeters

2.2.1 History –Introduction to pulse oximetry

A pulse oximeter was first built in the 1930s to measure the oxygen content in humans [27]. It was built by Carl Methes in 1935 and measured blood oxygen saturation *in vivo* by transilluminating tissue [28]. This oximeter however was not able to distinguish between arterial and venous (and capillary) blood. In an attempt to include this feature of distinguishing arterial and venous blood, two methods were introduced. The first being zeroing the oximeter by taking a 'bloodless' reading from an earlobe compressed between two fingers and the second arterializing the blood by heating it to 43°C which was developed and introduced during the Second World War as part of a project to investigate the problem of the loss of consciousness by R.A.F. pilots during dogfights. It was however found out that, the transmitted light through the finger or earlobe was not only attenuated by the arterial, venous and capillary blood but also by the skin (whose pigmentation and absorption

properties will vary from individual to individual) and by other tissues including the muscles and the bone.

In 1940, Glen Millikan came up with name, “oximetry” to describe a device he had innovated that was lightweight. Later in the 1940s, Earl Wood used pulse oximeters similar to that of Millikan in the operating room and in 1950, innovated a modification of Millikan’s invention that was used in numerous clinical and laboratory investigations at that time.

The Hewlett−Packard company in the early 1970s developed an instrument which attempted to eliminate these problems by measuring the transmission of light across the earlobe at more than two wavelengths. However, this innovation came along with high instrumentation costs and the need take measurements with eight varying wavelengths and so never found its use in the health industry.

Fast forward to the mid-1970s, Japan engineer, Takuo Aoyagi, whiles developing a semi-non-invasive technology to estimate cardiac output by detecting the washout curve of dye, injected into a peripheral vein as it diffused through the ear realised that he could build an ear pulse oximeter that measured arterial haemoglobin. This was one of the first inventions that was marketed in the mid-1970s. Further alterations and modifications were done in the late 1970s and early 1980s by Scott Wilber and William New respectively, that have led to the basis of this non-invasive technology in modern health care.

2.2.2 Existing Pulse Oximetry Innovations

Pulse oximetry has seen varying and innovative modifications to initial inventions and ideas over the years. Most scientists and researchers have started exploring the reflectance mode of Photoplethysmography and improving its accuracy to match that of the transmittance mode [29], [30]. Other pulse oximeters are self-sufficient and exist in one unit casing while others still depend on the use of wires for connecting to monitoring devices

like the pulse oximeters used for neonates in the Intensive Care Units (ICUs). Others have also been innovative and adopted wireless communication modes for sharing data and pulse readings [31]. Most pulse oximeters are now made into wearable devices like watches and are sometimes integrated into other technologies like mobile phones and watches [32], [33].There are also advanced pulse oximeters which are used for remote monitoring and management [34]. Pulse oximeters for neonates have also advanced over the years. Most of these technologies are integrated into monitoring devices and usually the ones used for neonates in ICUs and homes have the pulse sensors connected with wires to a monitoring device [35]. Some pulse oximeters have been made into headbands [36], [37], bodysuits with sensors [38], and even socks [39].

2.2.3 Review and Limitations in existing solutions

Pulse oximeters even though being a very innovative invention in modern healthcare systems still possesses some setbacks that prevent it from attaining its total usefulness. Some of these setbacks include the effects of the interference of ambient light, skin pigmentation, dyshemoglobinemia, low peripheral perfusion states, and motion artifact [40]. These setbacks can reduce the accuracy, clinical confidence, and application of readings for further diagnosis and studies. Some of the setbacks like the interference of ambient light could be eliminated by using a suitable covering or casing which prevents ambient light from having access to the pulse sensor element. According to research, dark skin pigmentation results in overestimation of arterial oxygen saturation, especially at low saturation [41]–[43]. Apart from the above listed limitations, some neonatal pulse oximeters are bulky with wires connected to external monitoring devices and others which have different sensor components are non-reusable because of the material used for the strap for the sensor. Other pulse sensors too have been found to cause burns after prolonged attachment to a neonate's skin [44], [45]. However, this is a rare and avoidable occurrence in pulse oximetry.

2.3 Analogue and Digital Pulse Oximeter Design Approach

The design and build of pulse oximeters can take a typical analogue or digital approach. The major differences between these approaches are power efficiency, building topology and cost of building.

The analogue approach solely filters and amplifies the signals in the analogue domain before preparing it for sampling by the ADC and further computations with the microcontroller. For the analogue approach, the red and infrared light signals are received by a photodetector like the photodiode which converts the light signal transmitted to current. A current-to-voltage converter which is usually, a differential current-to-voltage converter is used to convert the current from the photodiode into voltage. This voltage is also amplified with external interferences like ambient noise but due to the positive and negative signals produced by the differential amplifier, which can be passed through a single-ended amplifier, the noise or interference can be cancelled out. A sample and hold circuit is then used to separate the respective red and infrared signals since only one photodetector is used and both signals were initially combined as one. These separated signals are now filtered and amplified individually so that the signals would have the same phase and gain. These signals now consist of a very large DC component and a very small AC component which is about (0.5 to 2 percent) of the DC component. An offset amplifier is used to remove the DC component and the AC signal is amplified and received by the ADC of the microcontroller for sampling and further computations. A multiplexer, followed by sample-and-hold circuitry, is used to determine whether the filtered red or infrared signal is to be considered by the ADC.

For the digital approach, some filtering is done in the analogue domain and additional filtering in the digital domain before sampling and computations take place. The

system is same as the analogue approach till the current to voltage conversion. After this stage, analogue signal conditioning takes place using filters and amplifying circuits. Further filtering takes place in the MCU before sampling and then computations. A DAC or PWM is often used to control the intensity of the LEDs and used as an offset to properly condition the signal to meet the ADC's specifications.

The analogue approach has much bulkier outlook than the digital because it uses more op-amp circuits for most of the analogue signal processing, and the MCU for timing and the needed calculations. This approach also requires less power consumption by the MCU since most power is consumed in the op-amp circuits. The digital approach however depends on the MCU for almost everything including further filtering, switching and light intensity control and thus draws a lot of power. In other to suffice for the high consumption of power by the MCU, a highly capable MCU requiring low power would have to be used. There are a lot of such MCUs existing in the technology space in this modern era.

Chapter 3: Design

This chapter lays out the requirements for the proposed solution. The requirements in this section would include the user requirements and the design requirements. The proposed solution in order to be implemented will have both hardware and software subsystems that will communicate with each other. Thus, the design requirements are further subdivided into hardware and software requirements.

3.1 User Requirements

Below are some of the user requirements in response to the problem presented

- The device should be lightweight and have a lesser number of wires to reduce the bulkiness and size of device
- The device should be reusable
- The device should be low cost and affordable
- The device should not pose danger such as burns to neonates
- The device should not require a monitoring device to display readings
- The device should require low direct current (DC) voltage supply

3.2 Design Requirements

The design requirements needed to properly implement this project include the following.

3.2.1 Hardware requirements

The hardware requirements presents both electrical and mechanical design requirements which include:

- a transmittance pulse sensor design approach

- a system capable of operating at extremely low frequencies since the blood flow in the body occurs at frequencies even lower than 10 Hz.
- low energy-consumption microprocessor with high performance data processing algorithms
- low dc supply voltage source
- dc supply should have a long battery life
- high storage capacity of the microprocessor
- filter design capable of removal of noise (ambient noise and dc offset)
- a small display with good lighting and contrast for displaying readings
- highly secure and safe pads to eliminate possibility of burns
- Non-toxic material for pulse sensor strap

3.2.2 Software requirements

- microprocessor should possess a high frequency with high performance data processing algorithms
- high error tolerance and accuracy
- the response time of pulse oximeter readings should be less than thirty seconds considering averaging of readings before display
- highly accurate digital signal processing algorithms for filter design

- the system should possess interrupt features over polling options
- software should be compatible and able to communicate with hardware components effectively
- displayed readings should be from the averaged measured readings

Chapter 4: Methodology

The design for the neonatal pulse oximeter consists of both hardware and software components. The hardware design, is subdivided into electrical and mechanical design. This chapter gives an in-depth overview of what each design section entails with the various components and parameters chosen and why they were chosen.

4.1 Block Diagram

The design of this neonatal pulse oximeter used a transmittance PPG approach and a digital design topology. The transmittance approach was chosen because it provided more accurate readings especially for neonates. The digital topology was chosen over the analogue because one of the objectives of this project is to make a less bulky and lighter device. Since the analogue approach requires more hardware components that would increase size and space needed for the device, the digital topology highly satisfies this important objective that exist as a gap in neonatal pulse oximeters.

This design consists of a pulse sensor which has a transmitting circuit consisting of a Red LED and an Infrared LED switched on alternately at a defined duty cycle and a receiver circuit which is basically a light intensity-to-voltage converter. The light intensity to voltage converter is an integrated circuit (IC) consisting of a photodiode that receives transmitted light signals and converts them into current and a trans-impedance amplifier that converts these small amperes of current into voltage and amplifies the signal. The light intensity-to-voltage converter IC was chosen over the combination of a photodiode and a trans-impedance amplifier due to the constraint of the size of the device. The signal then goes through a passive low pass filtering to eliminate the interference of ambient light of 60Hz. A DC removal circuit is implemented with a passive high pass filter to obtain the AC signal which is further amplified with a gain of 31 because the AC signals are approximately,

1 to 2 percent of the DC signal. For example, if the DC signal is 3.3 V, then the AC component will be around 33mV to 66mV. Amplifying the signal with a gain of 31 gives an AC signal of 1.02V to 2.05V which can be converted to digital signals by the ADC. After the analogue conditioning, two signals for AC and DC are picked and sent to two ADC channels of the microcontroller. The ADC converts the analogue signals to digital signals. The AC signals are further conditioned in the digital domain using digital signal processing features of the Microprocessor (MCU) to reduce baseline wander which hinders the detection of the wanted signals. Computations of the required readings are made with the help of the MCU and displayed on an OLED display. Pulse Width Modulation (PWM) from the MCU coupled with a transistor drive circuit is used to control the LED current and intensity. Figure 7 illustrates the block diagram of the system.

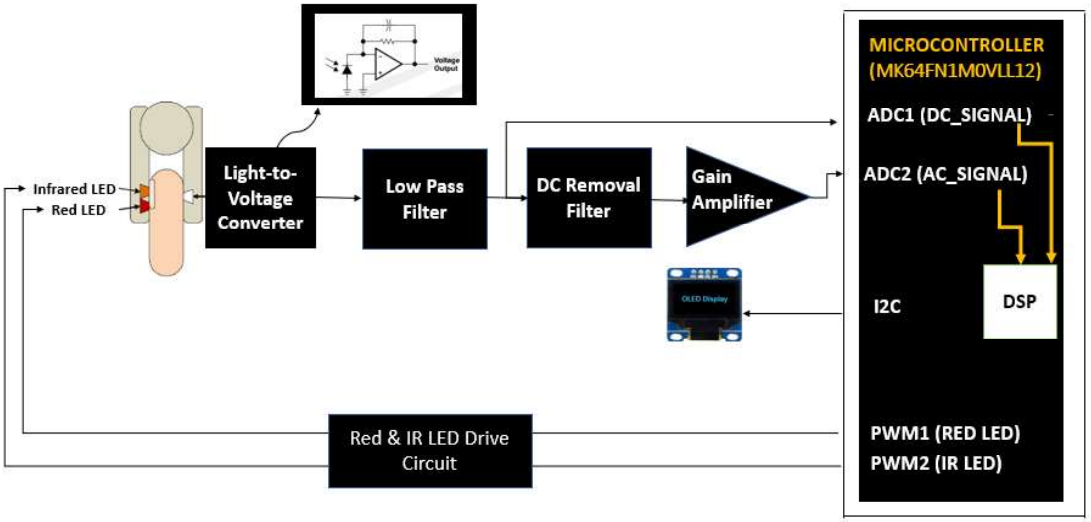

Figure 4.1: Image of the system's block diagram

4.2 Hardware Design

4.2.1 Electrical Design

In this design, the system is broken down into five sub-systems.. These include the power circuits, the led driver and sensor circuit, the analogue signal processing circuit, the control circuit which comprises the MCU and the display and the buzzer for interactivity.

Power Circuitry

The source of power for this device is one 12V A23S Alkaline Battery. This battery was chosen because of its small size and because it has a high energy density, longer shelf life and a longer battery life. This 12V voltage would be converted to an output voltage of 3.3V which is the optimal voltage for all the circuitry and components needed for building this device. A LD1117V33 low dropout voltage regulator was used for this step-down of voltage. It can step any voltage down within the range of 4.3V to 15V. Using the LD1117V33 voltage regulator requires a 100nF filtering capacitor at the voltage input and 10uF capacitor at the voltage output to maintain a constant DC value by removing power ripple as much as possible. A 1n4007 power rectifier diode is used in this case not for rectification but to ensure the flow of current in one direction and strictly restricts current from flowing in the opposite direction. 0.1 µF capacitors are also used as decoupling capacitors at the voltage outputs of the voltage regulator to the voltage inputs of the required circuitry. This system supplies power to the Led drive circuit (LDC), the OLED display, the MCU and the Light to Voltage Converter (LVC). The power circuit has a rocker switch which is used to turn on or off the power system.

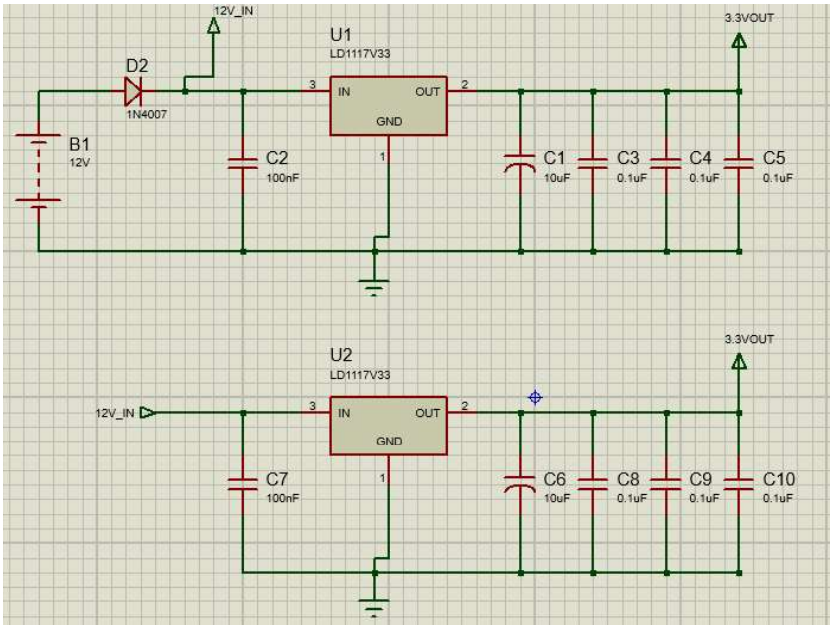

Figure 4.2: Image of the power circuitry

The Led Drive Circuitry (LDC) and Pulse Sensor

The LDC consists of a dual Single Pole Double Throw (SPDT) switch (ADG884BRMZ) and NPN BJT transistors (2N3904) in this case used as switches. It receives two pulse width modulations from the MCU to drive the LEDs alternately since only one photodiode is used in this system.

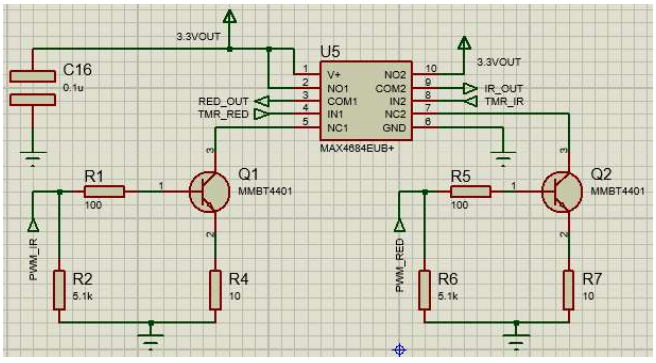

(a)

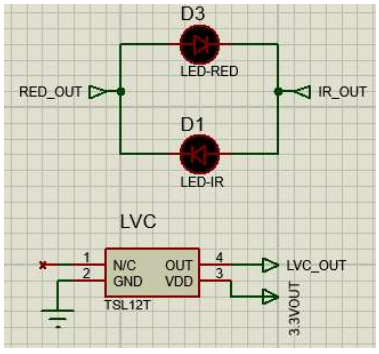

(b)

Figure 4.3: Image of the (a) LED Drive Circuitry (b) Pulse sensor circuit

The pulse sensor consists of the Red and Infrared LEDs and a light to voltage converter which is a combination of a photodiode which converts light intensity to current and a transimpedance amplifier which converts some milli amperes of current to some millivolts. The red and infrared LEDs chosen were LTL-4266N and WP7113SF6BT-P22 respectively. These were chosen because of their size, maximum current and their wavelengths. The light to voltage converter chosen was TSL 12T due to its ability to detect wavelength within the range of 320 nm to 1050 nm which included the wavelength of the red (600- 750 nm wavelength) and infrared LED (850-1000 nm wavelength) needed to be detected.

Analogue Signal Processing Circuitry

This circuitry consists three main stages. The first stage is a passive low filter, with a 3 dB cut-off frequency of approximately 60Hz to attenuate ambient noise. The second stage is a dc blocking stage to remove dc components and a this is typically a high pass filter with frequency of approximately 0.3Hz. The next stage is a gain amplifier with a gain of 31 to amplify the ac signals. The computational designs of the three stages of this circuitry are explained below.

Passive Low Pass Filter Design

Equation 16

$$f_c = \frac{1}{2\pi RC} = \frac{1}{2\pi X 268\Omega X 10\mu F} = 59.39\text{Hz}$$

Cut-off frequency required (f_c) = 60Hz

Resistor value (R) = 268 ohms = two 100-ohms resistors + 1 68-ohm resistor

Capacitor value (C) = one 10µF capacitor

Passive High Pass Filter Design (DC blocking)

$$f_c = \frac{1}{2\pi RC} = \frac{1}{2\pi\ X\ 510K\Omega\ X\ 1\mu F} = 0.312\ \text{Hz}$$

Cut-off frequency required (f_c) = 0.3Hz

Resistor value (R) = 510K ohms = one 470K-ohms resistor + two 220k-ohms resistors

Capacitor value (C) = one 1 µF capacitor

Gain Amplifier

Equation 17

$$Gain\ (A) = -\frac{R_f}{R_I} = -\frac{147k\Omega}{4.7k\Omega} = -31.28$$

Feedback Resistor value (R_f) = 147K ohms = one 100K-ohms resistor + one 47k-ohms resistors

Input Resistor value (R_I) = 4.7K ohms = one 4.7K-ohms resistor

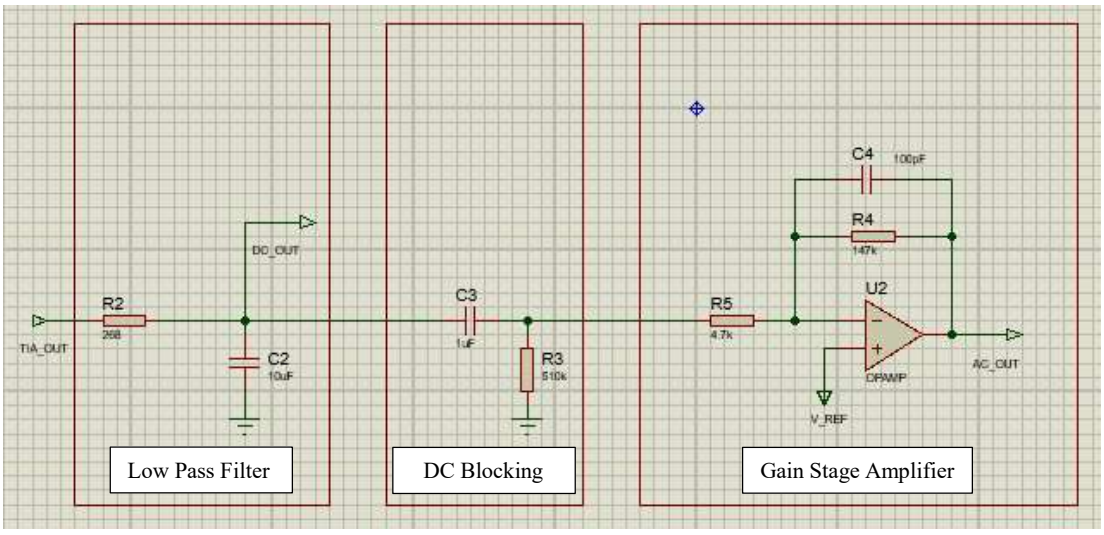

Figure 4.4: Image of the Analog Signal Conditioning Circuitry

Microcontroller Unit (MCU)

The Microcontroller unit used for this project is the MK64FN1M0VLL12 from the Freedom Board FRDM K64F. The digital approach chosen for the design of this pulse oximeter requires a low power, yet very capable MCU which also possesses digital filtering and digital signal processing capabilities. The MK64FN1M0VLL12 MCU has an Arm® Cortex®-M4 Core which is a highly efficient embedded processor.

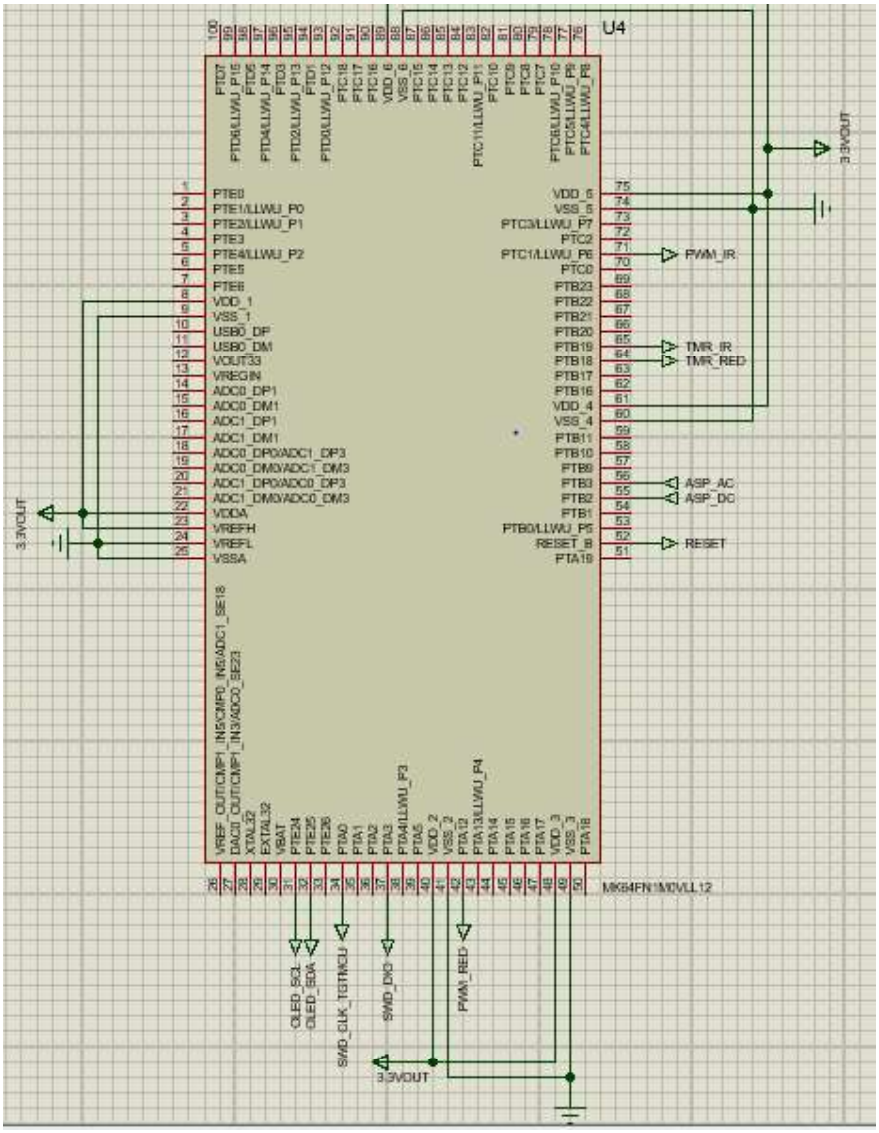

Figure 4.5: Image of the control circuitry

MCU Selection

The selection of the MCU was based on the criteria listed in the table below. From the Pugh chart in Table 4.2, both MCU choices had the same weightings. The MK64FN1M0VLL12 MCU was thus chosen since its board was readily available for prototyping purposes.

Table 4.1: Some operating features of MK64FN1M0VLL12 and STM32F446

Criteria	**MK64FN1M0VLL12 from the FRDM-K64F Development Board (Arm® Cortex®-M4 Core)**	**STM32F446 (Arm® Cortex®-M4 Core)**
DSP Embedded Feature	Using CMSIS Library	Using CMSIS Library
Program Memory Size	1MB (flash type)	512KB (flash type)
Operating Frequency	120 MHz (Max)	180 MHz (Max)
Operating Voltage Range	1.71 -3.6V	1.8 – 3.6V
Communication Interfaces	3 I2Cs, 3 SPI, 6 UART	3 I2Cs, 4 SPI, 2 UART
Cost	$ 20.90	$14.9
Dimensions (Size)	(20 x 20 x 1.6) mm	(3.82 x 3.728) mm

Table 4.2: Pugh chart for MCU selection

Criteria	Weight	Baseline	MK64FN1M0VLL12	STM32F446
DSP Embedded Feature	1	0	+1	+1
Program Memory Size	1	0	+1	+1
Operating Frequency	1	0	+1	+1
Operating Voltage Range	1	0	+1	+1
Communication Interfaces	2	0	+1	+1
Cost	2	0	-1	+1
Size/ Dimensions	2	0	+1	-1
TOTAL			**+6**	**+6**

Display/ Interactivity

To display the results of the pulse rate and oxygen saturation levels, an OLED I2C display screen was chosen because of its small screen size (22 X 11mm) and its high pixel resolution (128X64 pixels) with embedded backlight.

4.2.2 Mechanical Design

One of the major objectives of this project was to make the pulse sensor reusable as compared to the cloth-like and plaster ones used in other pulse sensors which are not reusable. The material used for the flap for this project is a silicon material which is reusable. For prototyping, the Thermoplastic polyurethane (TPU) was used to print a 3D model of the flap designed. The TPU material was used for printing because of its biocompatibility and

non-irritability with the human skin. Due to this reason, it is used for most non-invasive medical devices. The TPU is an inert material and just like other plastics becomes toxic when heated to a temperature of 428F degrees according to the TPU Material Safety Data Sheet [46]. The flap is 15cm long and 2 cm wide.

4.3 Software Design

4.3.1 System Clock, Crystal and MCU Code Upload

The FRDM K64F development board possesses a multi-clock generator (MCG) and an 48MHz internal reference clock (IRC48M) which are suitable for this application. The MK64FN1M0VLL12 possesses a crystal-less USB operation and is an example of the Kinetis MCUs that possess this feature [47]. This means that, the MCU's operation does not require an external crystal. In addition, this feature benefits the 48MHz internal reference clock which is used in this design.

To load code unto the MCU on the Printed Circuit Board (PCB), three header pin inputs were added unto the PCB. These include RST_TGTMCU which is connected to the RESET of the MCU, SWD_CLK_TGTMCU connected to pin PTA0 and SWD_DIO which is connected to the pin PTA3.

4.3.2 Timers and Pulse Width Modulation (PWM)

The Flexible Timer Module which is a 16-bit counter would be used for this application. Two timers with PWM are used for the alternate switching of the Red-IR and IR LEDs depending on a specified duty cycle. Timer 1(TMR_RED) is FTM2_CH0 (PTB18) and timer 2 is FTM2_CH1 (PTB19). Timer 1 is used for switching on the Red LED and Timer 2 (TMR_IR) is used for switching on the IR LED. A duty cycle of 11 per cent is initiated with a period of 2ms. This is to ensure maximum power savings from the supply. A 20.9MHz frequency is used with a prescaler of 2^7 (128), a channel value of 36 and a mod

value of 327. The PWM aids in the control of the intensity of the LEDs. Two interrupts are introduced to initiate the switching for each LED with a delay of 320us in between the switching of the red and IR LED for reading ADC values.

4.3.3 Interrupts

Interrupts are included in this design for the alternate switching of the RED and IR LEDs using PWM and Output capture. When the channel flag is raised for the channel value for the switching of the RED or IR LED, the ADC values for the red and the IR AC and DC values are read. After the AC and DC analog values are converted to digital values, the conversion complete flag is raised to initiate the digital signal processing.

4.3.4 Analogue-to-Digital Conversion (ADC)

The analogue-to-digital conversion of the DC and AC component of the received signals is done on two single-ended ADC input channels separately. The 16-bit analog-to-digital converter (ADC) is a successive approximation ADC. ADC0_SE12 is used for the conversion of analogue DC data and ADC1_SE14 is used for the conversion of analogue AC data.

4.3.5 I2C Organic Light Emitting Diode (OLED)

The OLED used in this prototype is an I2C serials communication protocol. An SPI OLED can also be an alternative for this application. The Serial Clock Pin (SCL) and Serial Data Pin (SDA) channels used for connection of the OLED are I2C0_SCL and I2CO_SDA respectively. The I2C0_SCL is the clock signal which will synchronize the data transfer between the MCU and the OLED and the I2CO_SDA will carry the data.

4.3.6 Program Flow Chart

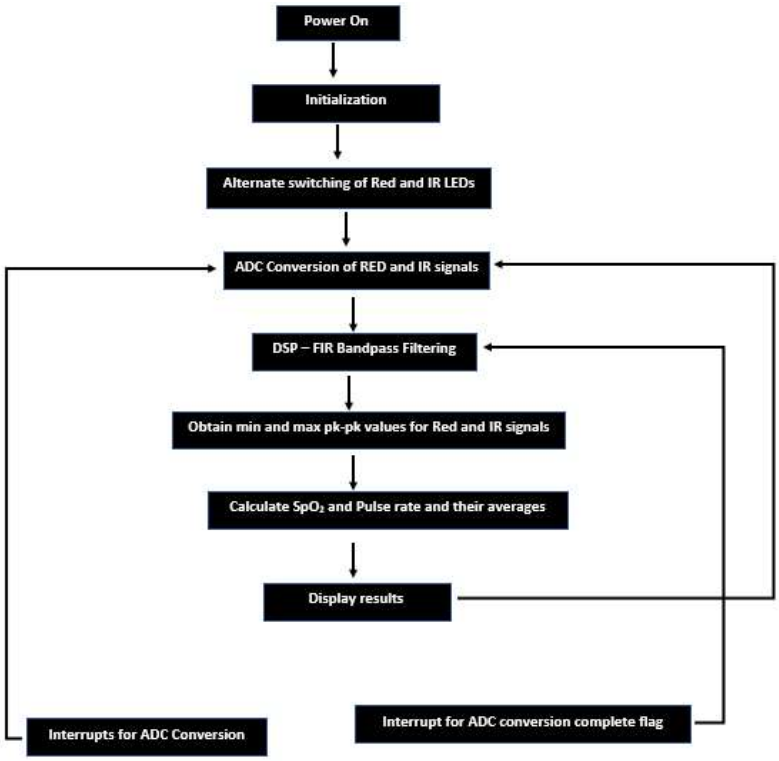

Figure 4.6: Image of program flow chart of system software

4.4 Design of Digital Signal Processing using MK64FN1M0VLL12

The output of the analogue signal conditioning circuit is connected to the ADC module of the MCU. During each LED's on-time period, one ADC sample is collected, and one ADC sample is taken during each LED's off-time period. Using the DSP feature of this MCU, a digital FIR bands filter is digitally built to filter the ADC data. This filtered data is then used to for the further computations for the parameters required. Below are the bandpass filter specifications which will be used to obtain filter parameters or co-efficients using MATLAB which will then be used in the code for the filtering. These specifications were obtained from Microchip's open-source FIR band pass filtering for accurate Pulse Oximeter readings [48].

Table 4. 3 FIR band pass filtering parameter specifications

Description	Specifications
Filter Type	FIR Bandpass
Filter Window	Kaiser Window
Lower Pass band Edge (w_{p1})	0.5 Hz (corresponding to 30BPM)
Upper Pass band Edge (w_{p2})	5 Hz (corresponding to 300BPM)
Lower Stop band Edge (w_{a1})	0.05 Hz
Upper Stop band Edge (w_{a2})	25 Hz
Sampling Frequency (w_s)	500 (Hz)
Passband Ripple (A_P)	0.1 (dB)
Stopband Ripple (A_a)	50 (dB)
Filter Length	513

The more critical transition bandwidth (B_t) for this filter is [0.45, 20] Hz and is calculated using the equation below and the corresponding values from table 3:

Equation 18

$$B_t = \min\left[\left(w_{p1} - w_{p1}\right), \left(w_{p1} - w_{p1}\right)\right]$$

The passband tolerance (δ_p) and stop band tolerance (δ_s) for this filter are 0.005 dB and 0.003 dB and are calculated using the equations below by change of subjects:

Equation 19

$$A_p = -20log_{10}\frac{1-\delta p}{1+\delta p}$$

Equation 20

$$A_s = -20log_{10}\frac{\delta s}{1+\delta p}$$

The fixed beta parameter (β) for the kaiser window which is a product of pi (π) and a parameter alpha that determines the shape of the window, is calculated with the appropriate

formular based on the stop band attenuation in dB. The stopband attenuation in this filter design was specified to be 50 and thus using the equation below, β was obtained to be 4.53.

Equation 21

$$\beta = 0.5842(A_a - 21)^{0.4} + 0.07886(A_a - 21) \text{ for } 21 \leq A_a \leq 50$$

This β parameter together with the other specifications in the table and calculated were used to design the filter in MATLAB and obtain coefficients using the "filterDesign" tool.

The FIR filter was selected because it is a stable type of filter, and it has a linear phase response. By changing the nth order Bessel function and manipulating the form factor with the adjustable parameter, α, the Kaiser window was chosen to lower the sidelobe level and control which most windows do not possess in DSP. The specifications for pulse rate in BPM have a range of 30-300. This corresponds to a bandwidth requirement of at least 0.5Hz-5Hz which was chosen for the pass band.

4.5 SpO_2 and Pulse Rate Calculations (BPM)

To calculate for SpO_2, two maximum and minimum peak values are obtained from the peak-to-peak output of the ASP_AC ADC for both RED and IR signals. The absolute value of the difference between the first set and second set of maximum and minimum values for both the RED and IR are found and averaged to get a peak-to-peak value for the RED (V_{pp_RED}) and IR(V_{pp_IR}). The V_{rms} values of the peak-to-peak values are then found by dividing the averaged peak-to-peak values by $2\sqrt{2}$. The V_{rms} values together with the DC value obtained from ASP_AC ADC for both RED and IR signals is used to calculate a ratio (R) using *equation 2*. This ratio with the help of a calibration curve as seen in figure 2.2 or a linearized equation in *equation 3* is used to estimate the SpO_2.

With a period of 2ms and a sampling rate of 500 hertz, beats per minute (BPM) pulse rate values are obtained by multiplying by 60 seconds all divided by the number of samples

between pulses using the IR LED. Two pulse rate values are calculated for when the number of samples between pulses is maximum (max) and when the number of samples between pulses is minimum (min). These two min. and max. pulse rate values are then averaged to obtain the heart rate in BPM.

4.6 Updated Prototype Design

Due to the unavailability of some of the specified electrical components used for the initial design including the specified voltage regulator, dual SPDT switch, light intensity-to-voltage converter, or a prescribed photodiode (PDB-C158) which are the basic components for building the pulse sensor, a new design was initiated for proof of concept. The updated design has a new power supply circuitry, a new LED Drive Circuit, and a new pulse sensing circuitry and a new light intensity-to-voltage converter.

The Updated Design for the Led Drive Circuitry (LDC)

To be able to create an effective current source for the pulse oximeter LED Drive Circuit, the Improved Howland current source topology [49] was used. This approach was chosen over other current source topologies because it is a very common and inexpensive method of creating a current source. This configuration employs the use of feedback resistors (R_F) that are scaled such that the common mode range of the inputs and the output current or swing limitations of the OPA is never exceeded. A set resistor (Rs) linearly modulates the current and can be tuned to help the output swing and reduce power dissipation. A transistor is not included in this LED Drive circuit because a huge amount of power is not required. This configuration would be used for two unidirectional controls through the excitation of two LEDs (Red and Infrared).

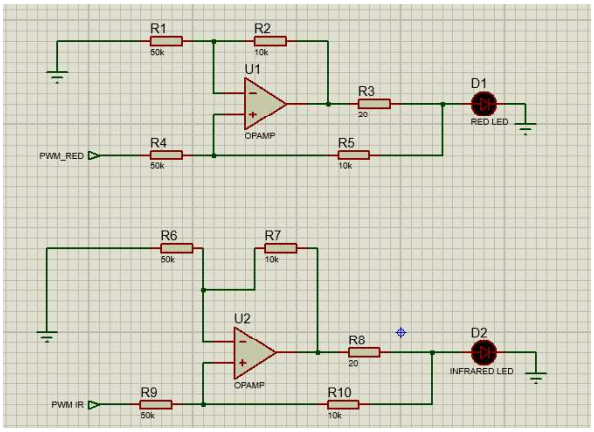

Figure 4.7 Image of the LED Drive Circuitry

The feedback resistors and set resistors were chosen based on the peak current desired and the voltage of the pulse supplied. This pulse oximeter has specifications for a low-current device and so a current less than 50mA was settled for. Using a pulse voltage of 3.3V and choosing R_F to be 10k ohms R_S to be 20 ohm and the input resistors R_I to be 10k ohm, a 33mA current was realised which met our specifications. The operational amplifier used was OP27.

Equation 22

$$I_{peak} = \frac{V_{pulse}\ X\ (\frac{R_F}{R_I})}{R_{set}} = \frac{3.3V\ X\ (\frac{10k}{50k})}{20} = 33mA$$

<u>The Updated Design for the Pulse Sensor</u>

The updated sensor only has an infrared LED and an OP999 photodiode. The OP999 is a silicon photodiode with average wavelength reception of 935nm thus only detects infrared light signals and not that of the red LED. Due to this limitation, only the pulse rate can be measured for this prototype. This is because, to calculate oxygen blood saturation, the ratio of red to infrared signals is used. The red light is significantly absorbed by deoxygenated blood whiles the infrared light is significantly absorbed by oxygenated blood.

The Updated Design for the Light Intensity-to-Voltage Converter

This circuit consists of the photodiode, OP999, and a transimpedance amplifier (TIA) circuit which converts the current from the photodiode based on a particular resistor value to voltage. The goal of this circuit is to convert an input current ranging from 0 to 33µA from the photodiode to an output voltage that ranges from 0 to3.3 volts. The available operational amplifier used was OP482 which is an JFET operational amplifier with a wide bandwidth of 4MHz which fits within this application. To be able to find the feedback resistor value for this conversion, the equation below is used. A capacitor value of 100pF is used to keep the TIA stable.

Equation 23

$$R_F = \frac{V_{oMAX-}V_{oMIN}}{I_{iMAX-}I_{iMIN}} = \frac{3.3V-0V}{33\mu A-0\mu A} = 100\text{k}\Omega$$

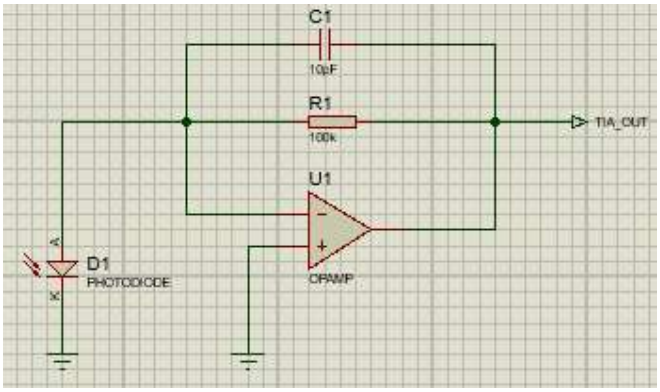

Figure 4.8: Image of the Transimpedance Amplifier Circuit

The Updated Design for the Power Circuit

The LM317 positive voltage regulator was used in place of the 3.3V regulator. A 3.3V source for driving components requiring this voltage was designed.

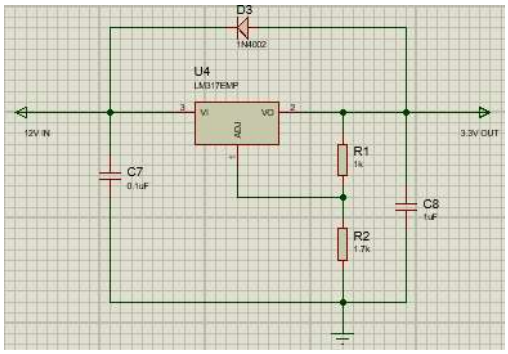

Figure 4.9 Image of the Voltage Regulating Circuit for 3.3V Supply

Chapter 5: Testing, Results and Discussion

This chapter presents how the various features of the proposed solution were tested, the results obtained and the implications of the results obtained. The results of the testing are expected to meet the design requirements for the system as stated in chapter 3.

5.1 Power Circuit

Due to unavailability of the 12V battery, a proteus simulation software was used for simulating the power circuit of the system. Digital voltmeter electrical components in the Proteus software were used for taking readings at the voltage test points for the input and output. A voltage of 3.3V was recorded after the voltage regulation stage and this meets the low power.

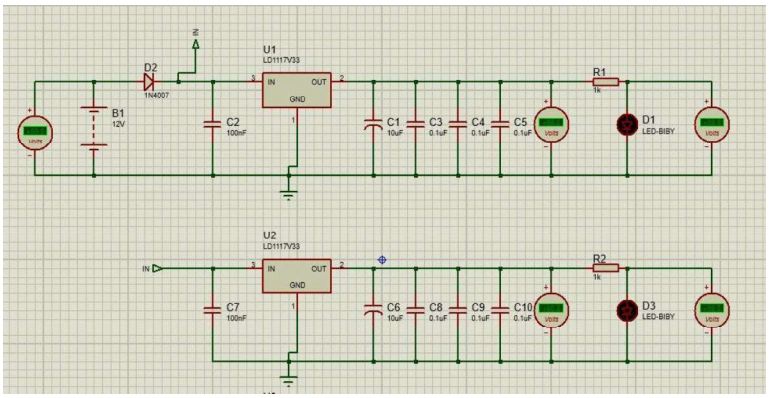

Figure 5.1: Image of power circuit simulation in the proteus software

5.2 Pulse Sensor Circuit

The pulse sensor's red and infrared LEDs were driven by two pulse width modulations with a period of 2ms and an on-time of 220us equivalent to a duty cycle of 11 percent. A period of 550us is initiated as a delay between the switching times of the red and infrared leds. The delay is necessary since only one photodiode is used and the two LEDs

being on at the same time would lead to errors in the photodiode current data. The oscilloscope of the NI ELVISmx instrument launcher with the NI myDAQ was used to ascertain the alternate switching of the LEDs corresponding to the required duty cycle (11 percent).

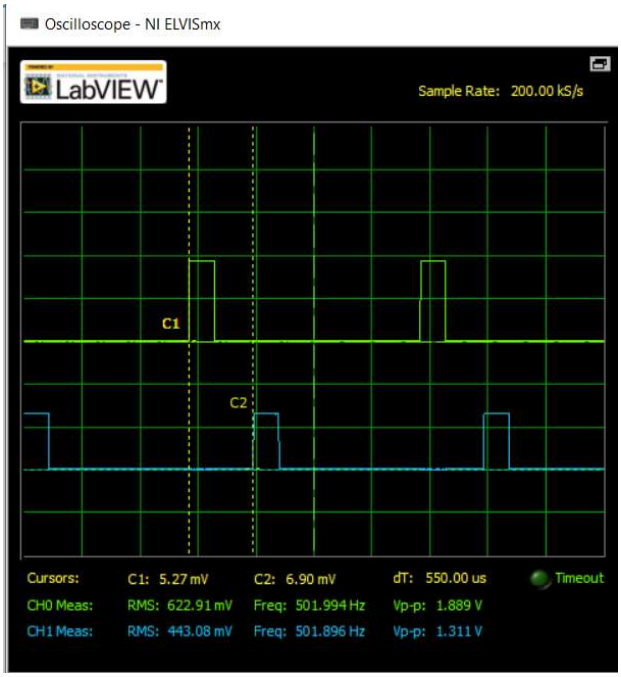

Figure 5.2: Timing diagram for the alternate switching of the RED (green) and IR (blue) LEDs

The current values obtained from the photodiode for the red and infrared LEDs when a finger is placed in between the transmitter and the receiver are summarized in the table below. The digital ammeter of the NI ELVISmx instrument launcher with the NI myDAQ was used for this measurement.

Table 5.1: Recorded current outputs for the detection of RED and IR signals by OP999

LED type	Lowest recorded current value (mA)	Highest recorded current value (mA)
Infrared	0.02	0.03
Red	0	0

The current values obtained from the photodiode for the RED LED is as a result of the photodiode which was available and used for this sensor. The IR LED (QED-123) and its photodiode (OP999) are from the DIGILENT Analog parts kit. As stated in chapter 4.6, OP999 has average wavelength reception of 935nm and can therefore not detect RED light signals. Thus, only the IR signal is sent to the transimpedance amplifier to be converted to voltage and further processed with the Analog signal processing circuit.

5.3 Analog Signal Processing Circuit

Using the NI ELVISmx digital oscilloscope and multimeter, the transimpedance amplifier output gave a voltage reading of 0.9V(900mV) for the DC reading and a value of 0.02V(20mV) for the AC voltage which is about 2.22 percent of the recorded DC voltage reading which was expected. Since the very large DC and the very small AC voltage are superimposed on each other, only the DC voltage component is clearly visualized here. The voltage for the AC was however confirmed using the digital AC voltmeter of the digital multimeter.

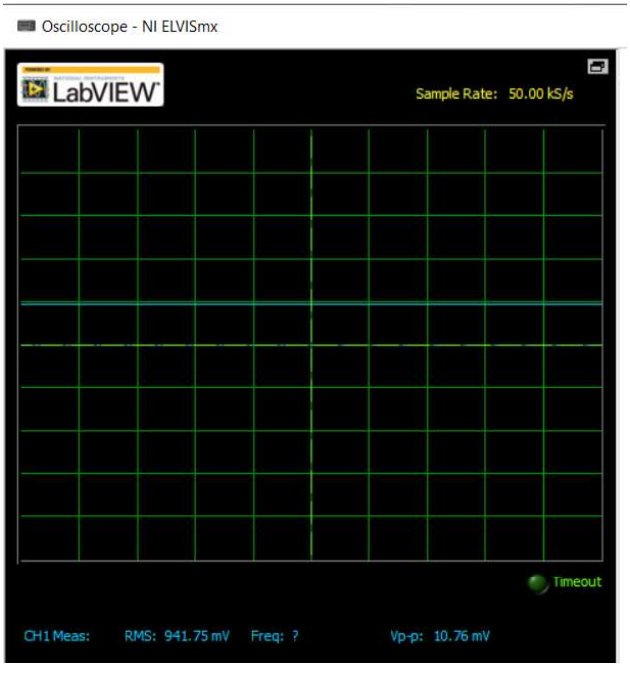

Figure 5.3: DC voltage plot for the output of the transimpedance amplifier

Th low pass filter designed gave a range of signals with a -3dB frequency of 59.57 Hz which is approximately 60Hz that it was designed for to eliminate ambient light of 60Hz. Below is the LabVIEW graph showing the magnitude and phase of the 60 Hz passive LPF designed.

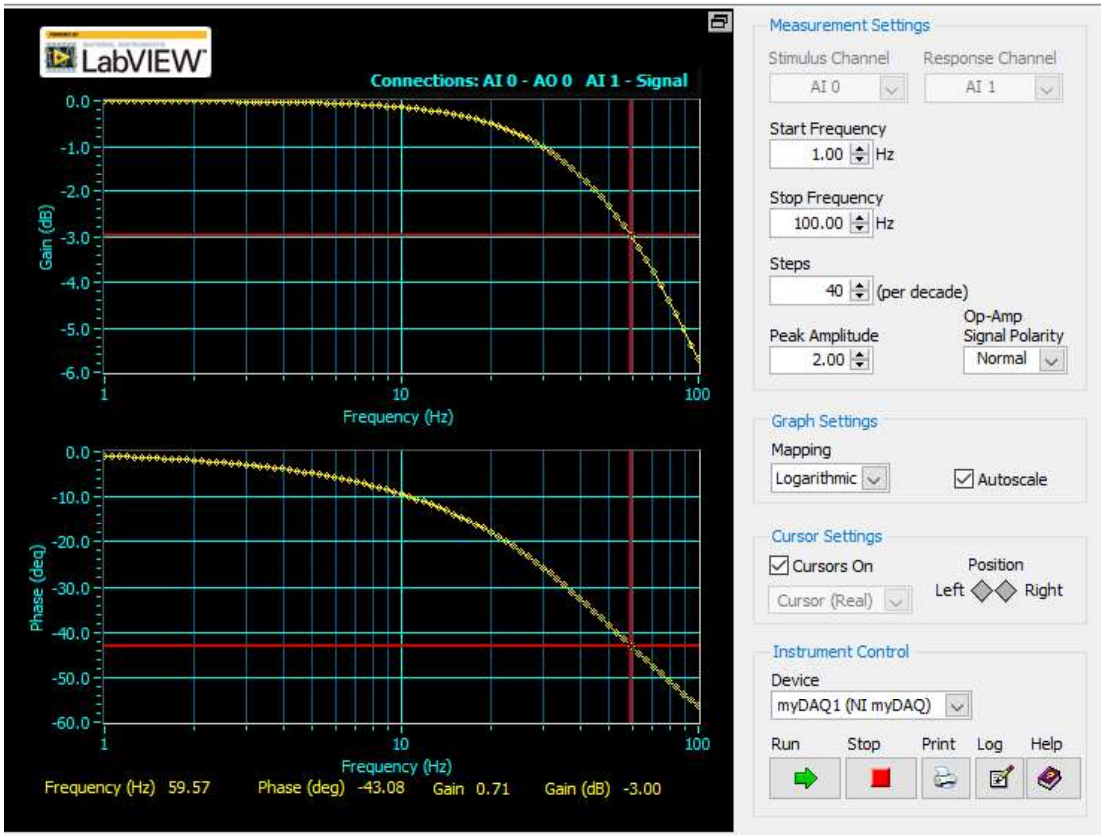

Figure 5.4: Bode plot of implemented passive low pass filter

To eliminate the DC component, a passive high pass filter with a cut-off frequency of 0.3Hz was designed. From the bode plot below, the -3dB cut-off frequency of the filter output is approximately 1.25Hz. This shift was observed because the minimum start frequency to use the bode plot is 1Hz and so the software could not visualize a cut-off frequency less than 1Hz. This would not however affect accuracy of the system since the recorded frequency is a low frequency corresponding to the low AC signals expected.

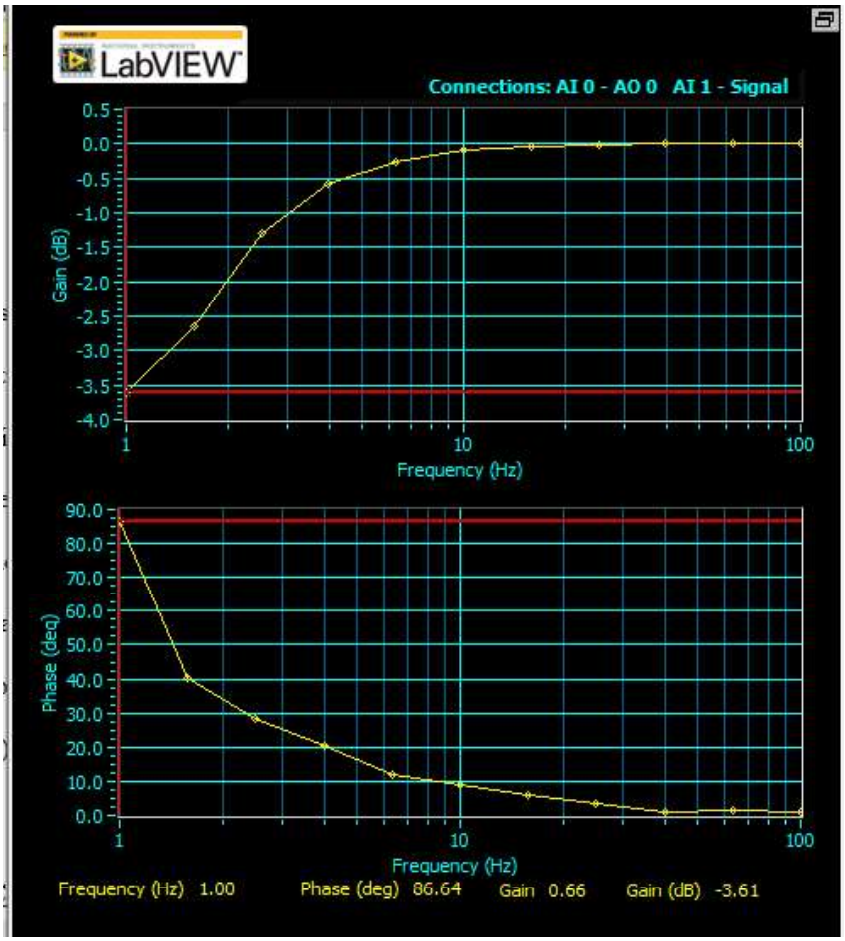

Figure 5.5: Bode plot of implemented passive high pass filter

A gain amplifying circuit was designed to increase the output of the minute AC voltages from the high pass filter. The oscilloscope plot below shows an increase of signals from 11.74mV to 41.73mV peak-to-peak.

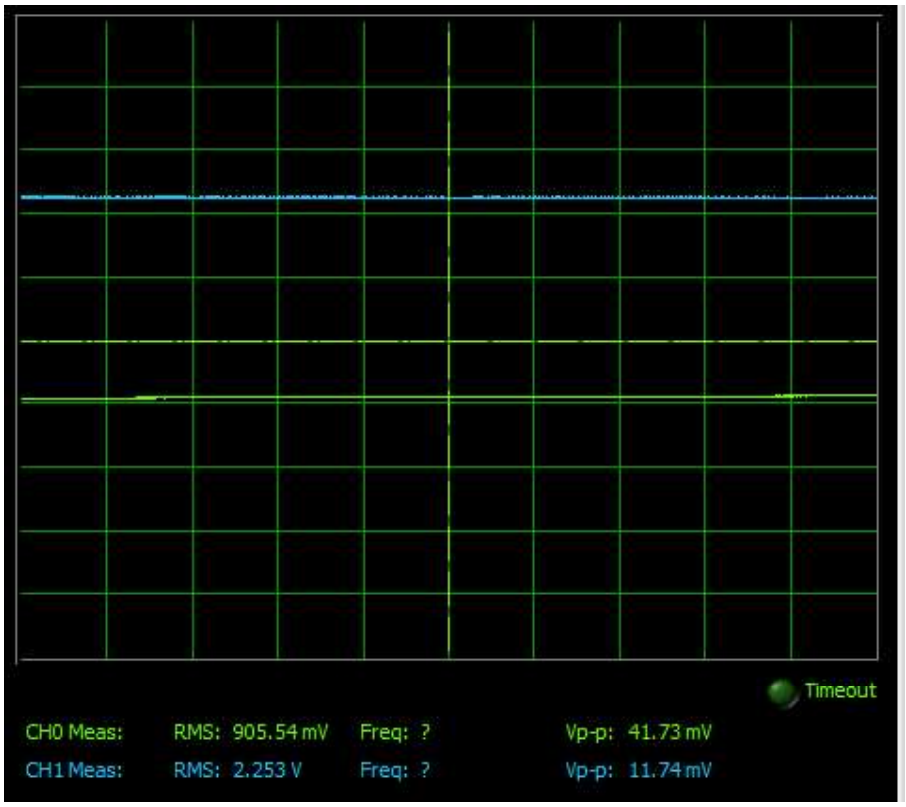

Figure 5.6: Plot showing output of gain amplifying circuit

5.4 Digital Signal Processing

In order to eliminate baseline wandering [50] of the PPG signals that would cause the interpretation of the signals to be difficult, a Finite Impulse Response (FIR) filter is used. The digital FIR band pass filter was first designed in MATLAB using the "filterDesigner tool" to obtain the filter coefficients for embedding into the MCUXpresso IDE software to filter the ADC values obtained from the Analog Signal Processing Circuit for the required frequency ranges. The filter length (co-efficient) obtained was 514, 32-bit unsigned numbers with an order of 513. For the Kaiser window used, a main lobe width of 0.17188 was realized with relative sidelobe attenuation of -13.4dB and a leakage factor of 0.06 percent. The sidelobe attenuation corresponds to the beta (β) parameter calculated in Chapter 4.4 and with an effect on the main lobe width. Based on these values and the plots below, we can conclude that the designed filter is a desirable one. With a leakage factor of

0.06 percent and a small main lobe width (0.17188), it ascertains that the transition bandwidth would also be small, resulting in a simpler filter occupying less space and with less delay time and less distortion, which is desirable.

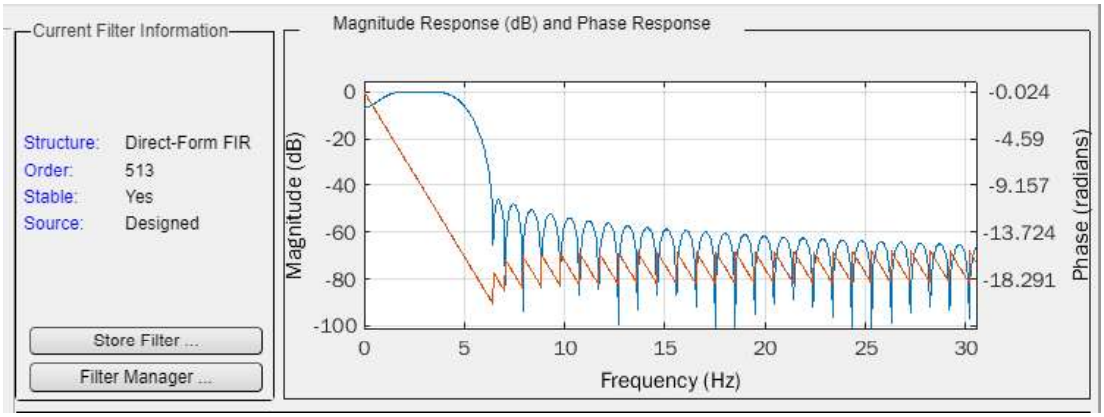

Figure 5.7: Bode plot of FIR bandpass designed

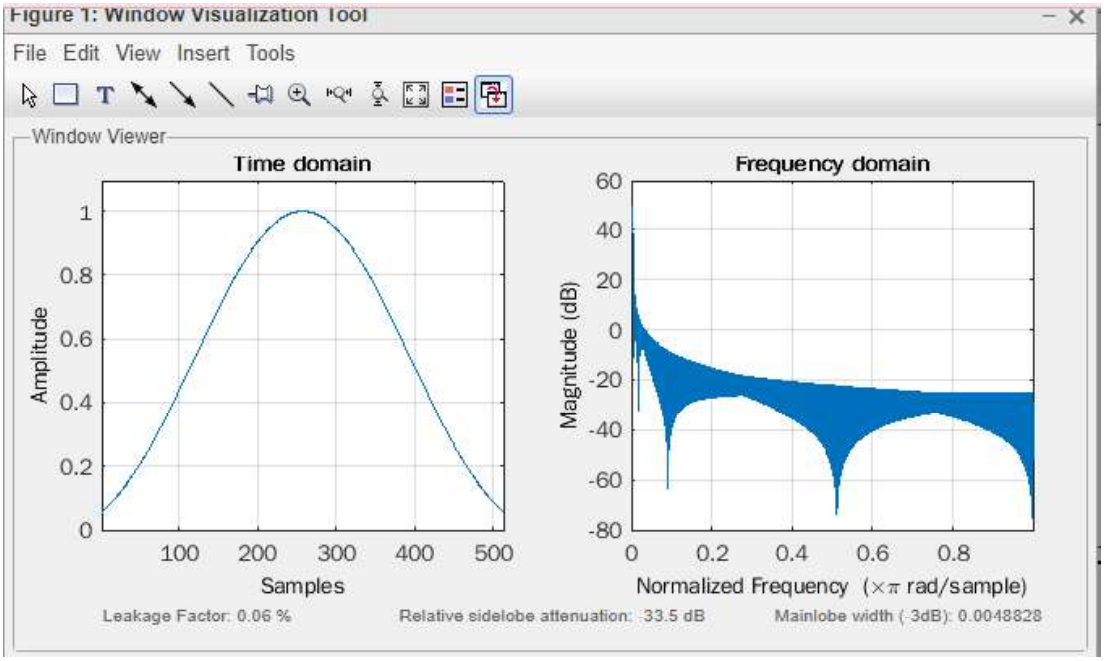

Figure 5.8: Time and Frequency domain plots of FIR filter outputs

Due to the difficulty in deploying the DSP feature using MCU Xpresso, a MATLAB algorithm was written for the deployment of the DSP and the pulse oximeter and the outcome of the DSP was visualized and analyzed. In addition, because of the new pulse sensor design which has a photodiode which can detect only IR signals and not red, only ADC IR values obtained from the MCU's ADC channels were analyzed with this method. Also, unfiltered PPG datasets were used to also ascertain that the DSP worked and also the algorithm for finding the SpO_2 and pulse rate in BPM were correct. Due to the unavailability of unfiltered PPG data for neonates, the unfiltered PPG dataset was obtained from the physionet database [51]for five healthy adults with age ranging from 20 to 53years with a mean age of 28.52 years who were in a sitting position and were used to assess the DSP validity. Ten thousand data points were obtained and used for each individual. Figures 5.9 and 5.12 are plots showing the effect of FIR bandpass filtering on AC ADC sampled IR and RED signals respectively. Each of this plot has three legends for three plots on a graph with the blue plot showing the unfiltered signal, the red showing the filtered signal and the green plot showing the desired range of the filtered signal based on the specifications in table 4.3. The plots in figures (5.10 and 5.11) and figures (5.13 and 5.14) gives a zoomed in view of the filtered signal and the filtered signal with its desired range for the IR and RED signals respectively. The graphs were plotted from 0 Hz to 20 Hz for the x-axis and amplitude for the y-axis.

From the graphs displayed below it can be seen that the unfiltered signals (blue) have noise superimposed on the desired signal. However, after filtering, the signals have the noise eliminated (red). It can also be visualized that the desired signal (green) ranges from 0.45Hz to 20 Hz which is the required critical transition bandwidth (B_t) calculated in chapter 4.4. This confirms that our FIR bandpass filter is effective.

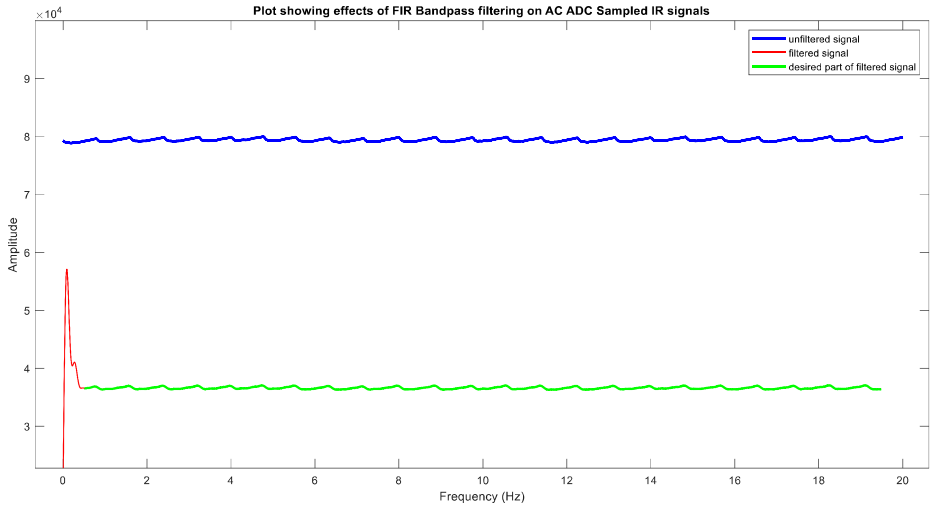

Figure 5.9: Plots showing the effect of FIR bandpass filtering on IR signals of Physionet dataset

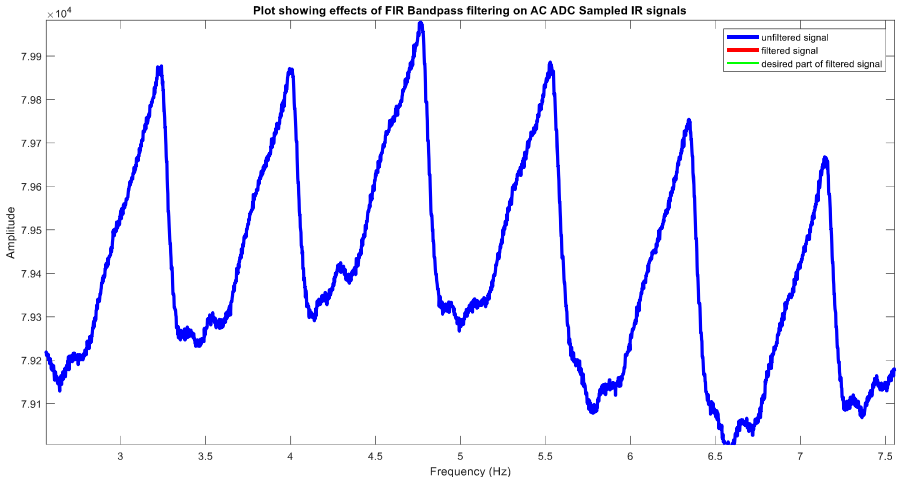

Figure 5.10: Plots showing unfiltered IR signals of Physionet dataset

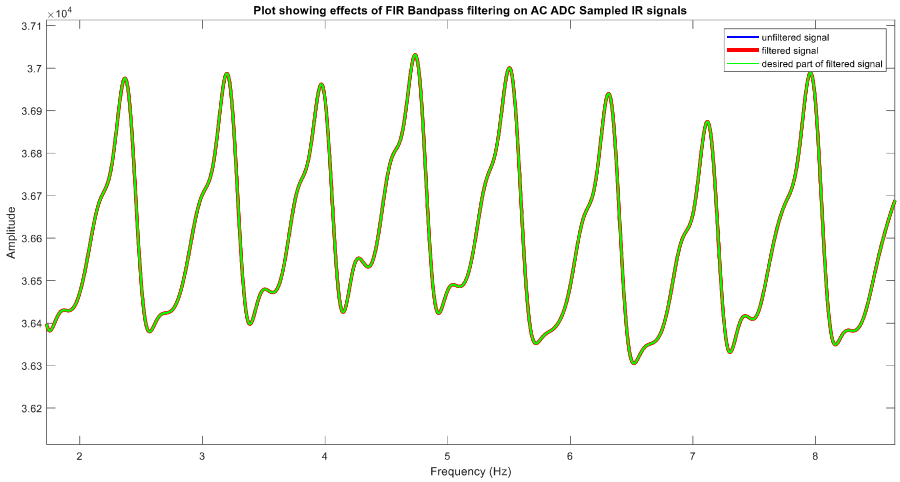

Figure 5.11: Plots showing filtered IR signals of Physionet dataset

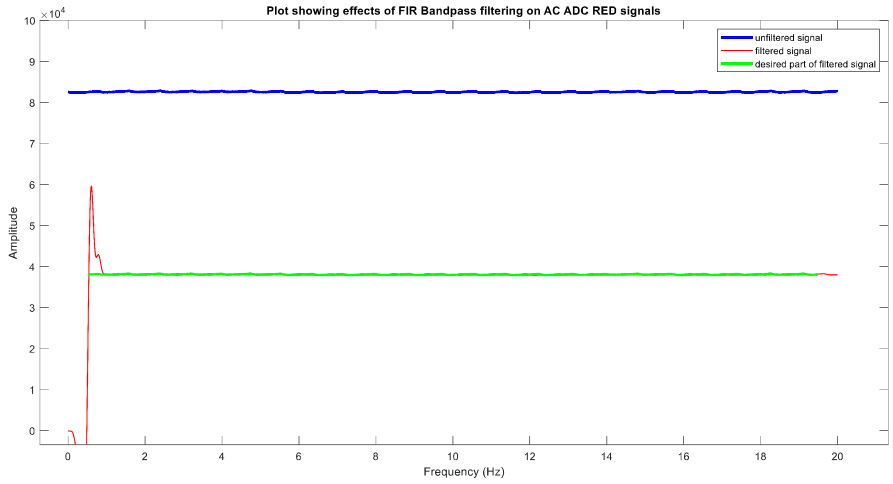

Figure 5.12: Plots showing the effect of FIR bandpass filtering on RED signals of Physionet dataset

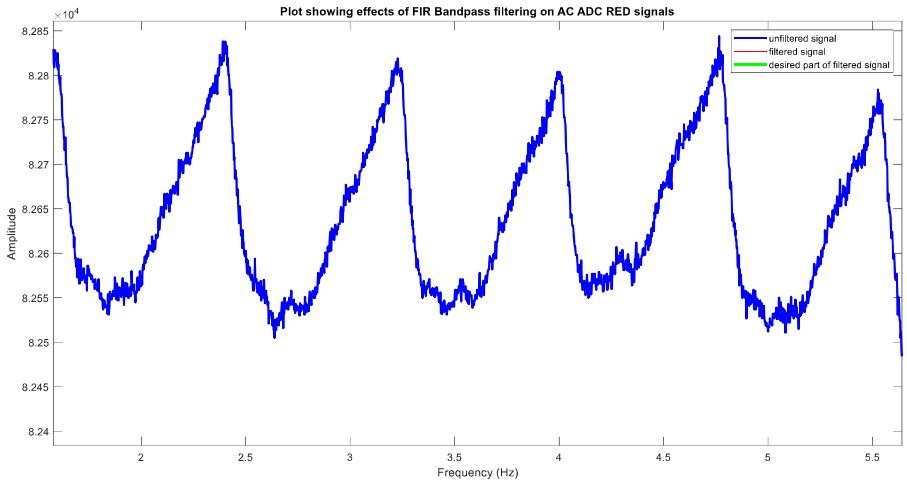

Figure 5.13: Plots showing unfiltered RED signals of Physionet dataset

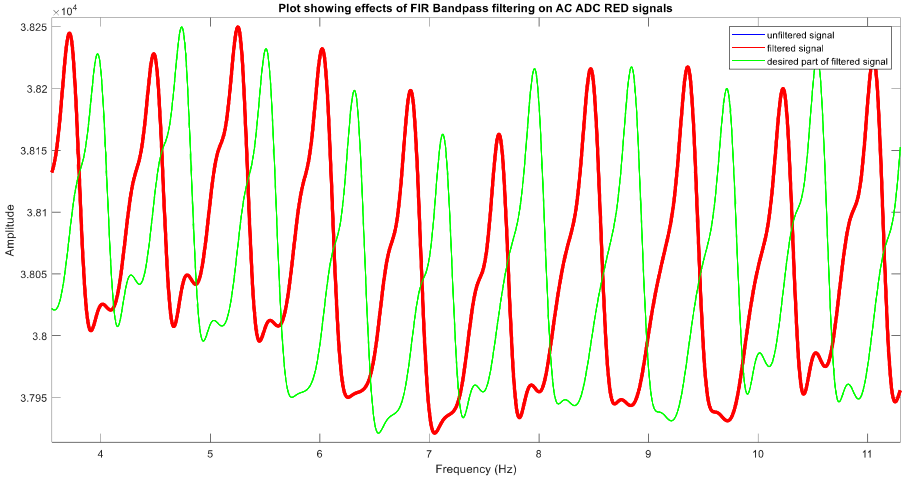

Figure 5.14 Plots showing filtered RED signals of Physionet dataset

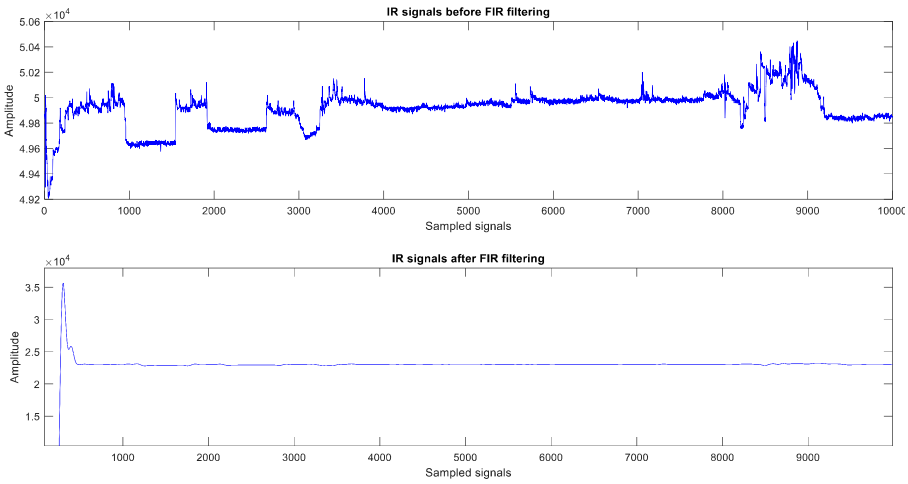

Figure 5.15: Plots showing the effect of FIR bandpass filtering on IR signals of the IR Sensor built

5.5 Pulse Oximeter Readings

The summary of the calculated pulse rate and SpO_2 readings for the physionet dataset can be viewed in the table below. Ten thousand datasets were obtained for each person (person 1 to person 5) sitting for readings at the distal phalanx (DP) and at the proximal phalanx (PP) for RED and IR signals. These were used to calculate the pulse rate and SpO_2 readings and then averaged to the values in the table.

Table 5.2: Summarized pulse rate and SpO_2 readings obtained using Physionet dataset

Peron no. & Contact location	SpO2 Avg. (%)	BPM Avg.	SpO2 Max (%)	SpO2 Min (%)	BPM Max	BPM Min
1DP	98	60.4656	107.3599	62.7141	60.4656	60.4656
1PP	95	61.0213	109.3123	35.9103	61.0213	61.0213
2DP	96	60.3214	109.424	43.8471	60.3214	60.3214
2PP	93	59.3188	109.3829	-92.2119	59.3188	59.3188
3DP	98	59.758	108.3348	20.0009	59.758	59.758
3PP	96	59.564	109.9443	20.489	59.564	59.564
4DP	98	60.1889	108.8974	-36.3048	60.1889	60.1889
4PP	94	59.6563	108.5781	-27.8673	59.6563	59.6563
5DP	94	60.362	109.4254	-338.0602	60.362	60.362
5PP	91	60.3238	108.8075	-87.523	60.3238	60.3238

The summary of the calculated pulse rate readings for the IR sensor sensor circuit built and the readings taken with the Lk87 fingertip Pulse Oximeter can be viewed in the data below. Both readings were taken using the left index finger of the student undertaking this research with approval from the Ashesi University's Institutional Review Board. Each reading in the IR Sensor-Built column is an averaged value of ten thousand values calculated pulse rate readings in BPM.

Table 5.3: Pulse readings from IR Sensor built and the Lk87 Pulse oximeter

Pulse Rate Reading No.	IR Sensor-Built (BPM)	Lk87 fingertip Pulse Oximeter (BPM)
Reading 1	78.6748	73
Reading 2	87.38	87
Reading 3	88.4493	89
Reading 4	80.1408	81
Reading 5	85.7925	85

Trendline plots were plotted to examine the trend in the values calculated and read using the Microsoft Excel software. From figures 5.16 and 5.17, it can be observed that, the number of plotted plots is equally distributed on both sides of the trendline drawn (dashed red lines). The obtained pulse readings and the trendline ascertains that the values read are almost within the same range. The obtained pulse rate readings also fall within the range for healthy adults which is from 60-100 BPM.

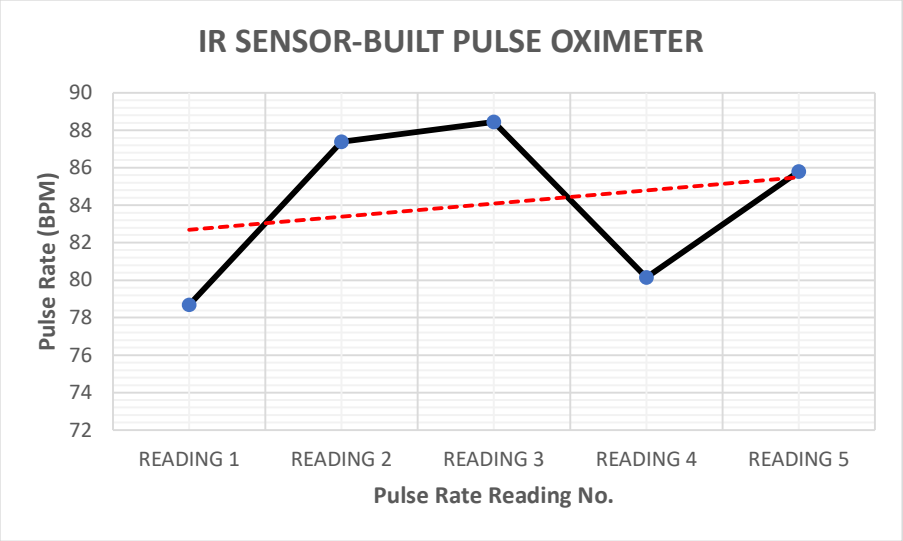

Figure 5.16: Pulse Readings for IR Sensor built

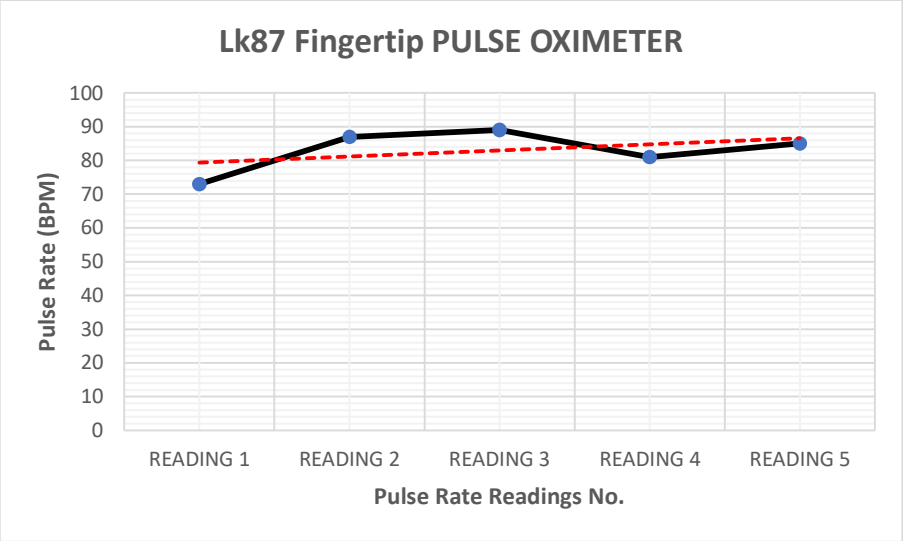

Figure 5.17: Pulse Readings Lk87 pulse Oximeter

5.6 Statistical Analysis

Assuming the dataset has a normal distribution, a two-sided paired T-test was conducted using the R software to determine if there is a significant difference between readings from the IR sensor built and the Lk87 fingertip pulse Oximeter. The initial hypothesis for the test was: H0: mean difference between the IR sensor built and the Lk87

fingertip pulse Oximeter is zero. A confidence interval of 95 percent was used for this test. The table below summarizes the results from the test.

Table 5.4: Results from the two-sided paired T-test

Paired T-test obtained parameters	Values
t-value	0.91738
Degrees of freedom (df)	4
p-value	0.4109
95 percent Confidence interval	-2.203764 and 4.378724
Mean difference	1.08748
Alternative Hypothesis	True mean difference is not equal to zero

The t-value obtained indicates that the readings obtained for both methods used in the test are similar because the t-value is small since the acceptable t-values range from -2 to 2. The p-value obtained indicates that the results obtained is not that far away from the null hypothesis stated above even though the alternative hypothesis states the mean difference is not equal to zero which is true. If the p-value was to be less than 0.05, then it confirms that the results obtained from this test is entirely different from the Null hypothesis stated which is no the case in this test. For a 95 percent confidence interval, we obtained a minimum and maximum difference of [-2.203764 4.378724] with a mean difference of 1.08748 meaning that 95 percent of a dataset produce these intervals which is a very good mean difference suggesting the two sets of readings are similar with no vast difference. This proves that the IR sensor that was built was effective and could be used for checking pulse rate.

Another plot in Microsoft Excel was plotted to visualize the similarities between the readings for the IR sensor built and the Lk87 fingertip pulse Oximeter. From this plot in addition to the statistical analysis, it can be concluded that the results obtained for both methods are not very different from each other.

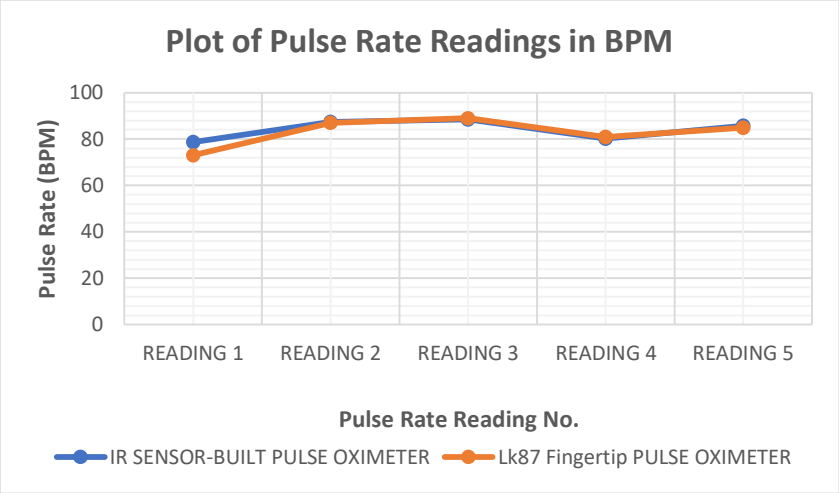

Figure 5.18: Graph showing similarity between IR sensor built and the Lk87 fingertip pulse Oximeter

5.7 Cost Analysis

One of the objectives of this design is to make it low-cost and affordable. One of the most notable pulse oximeter producers are Nellcor™. Displosable sensors from this company cost about 15 dollars per one and the cost of reusable pulse sensors cost about 70 to 250 dollars. These sensors are connected to a monitoring device to obtain the required readings and these devices' cost range from a 1,000 to 4,000 dollars [52].

Below is an estimated cost for building the designed neonatal pulse oximeter.

Table 5.5 Cost breakdown of building the proposed neonatal pulse oximeter design

Cost Description	Cost
Cost of required electrical components from bill of materials	Approximately $ 50
Cost of PCB printing	$ 5
Cost of 3D printing housing case for PCB and flap	$ 19.5
Total Cost	**$74.5**

This analysis confirms that the proposed design is a lot cheaper than a commercial neonatal pulse oximeter and would be of much benefit if implemented and commercialized.

Chapter 6: Conclusion

The first chapter gave an introduction to the problem and the limitations in the use of neonatal pulse oximeters. The chapters following focused on understanding the pulse oximetry space, defining a proposed solution, the needed requirements, the design and the implementation of the alternative design of a neonatal pulse oximeter. Due to some limitations in acquiring specified components and system problems, the pulse oximeter design was not able to be executed as a whole but rather in sections. In addition, because only infrared signals were received by the photodiode, only an IR sensor was built for pulse rate calculations. SpO_2 could not be calculated because it requires both RED and IR PPG signals. The sectioned results, discussions and statistical analysis confirms that the design is valid and the system works with a high similarity (t-value=0.917 in paired t-test) as a commercial pulse oximeter (Lk87 fingertip pulse oximeter).

6.1 Limitations

During the implementation of this design, there were three major limitations that were encountered.

- The specified TSL 12T light intensity-to-voltage converter (LVC) for the pulse sensor for the initial design was out of stock together with the other suggested replacements. The second design for the pulse sensor which suggested the use of a photodiode (PDB-C158) in place of the TSL 12T for detecting the RED and IR signals was also unavailable. Thus, an available photodiode OP999 which could only detect IR signals was used and thus, only an IR sensor was built.
- The implementation of the digital filter with the MCU proved difficult with a lot of errors after the filter co-efficient were obtained.

- Unfiltered PPG data for neonates was unavailable to be used to test the algorithm to obtain SpO_2 and pulse rate reading. This led to using an unfiltered PPG data for healthy adults even though for neonates would have been preferred since this pulse oximeter design was for neonates.

Talk about the lack of an appropriate photodiode to detect both red and IR signals.

6.2 Future work

The implemented design so far is feasible but would need to be improved to design a better prototype of the design. Some of these recommendations are below:

- Using the specified electrical components for the pulse sensor and analog signal processing circuitry
- Implementing the building of the printed circuit board design and putting it in the casing (kindly refer to appendix)
- Using the alternative MCU (STM32F446) when available for a much lower cost and ease in implementation of DSP since there is much more information and publications on using this MCU.

References

[1] E. D. Chan, M. M. Chan, and M. M. Chan, "Pulse oximetry: Understanding its basic principles facilitates appreciation of its limitations," *Respiratory Medicine*, vol. 107, pp. 789–799, 2013, doi: 10.1016/j.rmed.2013.02.004.

[2] C. D, E. A, G. M, S. C, and N. H, "A review on wearable photoplethysmography sensors and their potential future applications in health care," *Int J Biosens Bioelectron*, vol. 4, no. 4, 2018, doi: 10.15406/IJBSBE.2018.04.00125.

[3] "Kinetik Wellbeing." https://www.kinetikwellbeing.com/6-facts-everybody-should-know-about-pulse-oximeters/ (accessed Apr. 16, 2022).

[4] S. DeMeulenaere, "Pulse Oximetry: Uses and Limitations," *The Journal for Nurse Practitioners*, vol. 3, no. 5, pp. 312–317, May 2007, doi: 10.1016/J.NURPRA.2007.02.021.

[5] M. S. Engel and L. K. Kochilas, "Pulse oximetry screening: a review of diagnosing critical congenital heart disease in newborns," *Medical Devices (Auckland, N.Z.)*, vol. 9, p. 199, Jul. 2016, doi: 10.2147/MDER.S102146.

[6] P. Syamasundar, "Congenital Heart Defects – A Review," *Congenital Heart Disease - Selected Aspects*, Jan. 2012, doi: 10.5772/27002.

[7] N. E. Thomford *et al.*, "Clinical Spectrum of congenital heart defects (CHD) detected at the child health Clinic in a Tertiary Health Facility in Ghana: a retrospective analysis," *Journal of Congenital Cardiology 2020 4:1*, vol. 4, no. 1, pp. 1–11, Aug. 2020, doi: 10.1186/S40949-020-00034-Y.

[8] S. Liu *et al.*, "Association between maternal chronic conditions and congenital heart defects: a population-based cohort study," *Circulation*, vol. 128, no. 6, pp. 583–589, Aug. 2013, doi: 10.1161/CIRCULATIONAHA.112.001054.

[9] H. C. Aranguren Bello *et al.*, "Oximetry and neonatal examination for the detection of critical congenital heart disease: a systematic review and meta-analysis," *F1000Res*, vol. 8, p. 242, 2019, doi: 10.12688/F1000RESEARCH.17989.1.

[10] M. N. Plana, J. Zamora, G. Suresh, L. Fernandez-Pineda, S. Thangaratinam, and A. K. Ewer, "Pulse oximetry screening for critical congenital heart defects," *The Cochrane Database of Systematic Reviews*, vol. 2018, no. 3, Mar. 2018, doi: 10.1002/14651858.CD011912.PUB2.

[11] "NONIN 6000CI INFANT CLOTH DISPOSABLE SENSORS, BOX OF 24 (3 FEET / 1 METER)." https://www.turnermedical.com/NONIN_6000CI_INFANT_CLOTH_DISPOSABLE_SENSORS_p/nonin_6000ci.htm.

[12] “Pulse oximeter-associated toe injuries in a premature neonate: a case report - PubMed.” https://pubmed.ncbi.nlm.nih.gov/10634008/.

[13] Pa-psrs, “Patient Safety Advisory Skin Integrity Issues Associated with Pulse Oximetry,” 2005. [Online]. Available: www.psa.state.pa.us.

[14] J. L. Mildenhall, “The theory and application of pulse oximetry,” *Journal of Paramedic Practice*, vol. 1, no. 2, pp. 52–58, Nov. 2008, doi: 10.12968/JPAR.2008.1.2.42016.

[15] “Capnography And Pulse Oximetry - PubMed.” https://pubmed.ncbi.nlm.nih.gov/30969576/.

[16] “The Biomedical Engineering Handbook, Fourth Edition - Book Series - Routledge & CRC Press.” https://www.routledge.com/The-Biomedical-Engineering-Handbook-Fourth-Edition/book-series/HBI#.

[17] S. Brown, S. Liyanage, P. Mikrou, A. Singh, and A. K. Ewer, “Newborn pulse oximetry screening in the UK: a 2020 survey,” vol. 396, p. 881, 2020, doi: 10.1016/S0140-6736(20)31959-0.

[18] “Pulse oximetry: theory and applications for noninvasive monitoring - PubMed.” https://pubmed.ncbi.nlm.nih.gov/1525987/.

[19] “The feasibility of spectrophotometric measurements of arterial oxygen saturation from the fetal scalp utilizing noninvasive skin-reflectance pulse oximetry - PubMed.” https://pubmed.ncbi.nlm.nih.gov/1596651/.

[20] Y. Mendelson and M. J. McGinn, “Skin reflectance pulse oximetry: in vivo measurements from the forearm and calf,” *J Clin Monit*, vol. 7, no. 1, pp. 7–12, Jan. 1991, doi: 10.1007/BF01617892.

[21] J. Allen, “Photoplethysmography and its application in clinical physiological measurement,” *Physiol Meas*, vol. 28, no. 3, Mar. 2007, doi: 10.1088/0967-3334/28/3/R01.

[22] Webster G. John, “Design of pulse oximeters (eBook, 1997) [WorldCat.org].” https://www.worldcat.org/title/design-of-pulse-oximeters/oclc/228122017.

[23] A. Reisner, P. A. Shaltis, D. McCombie, and H. H. Asada, “Utility of the Photoplethysmogram in Circulatory Monitoring,” *Anesthesiology*, vol. 108, no. 5, pp. 950–958, May 2008, doi: 10.1097/ALN.0B013E31816C89E1.

[24] C. M. Gardner, “Transmission versus reflectance spectroscopy for quantitation,” *https://doi.org/10.1117/1.JBO.23.1.018001*, vol. 23, no. 1, p. 018001, Jan. 2018, doi: 10.1117/1.JBO.23.1.018001.

[25] T. G. Mayerhöfer, S. Pahlow, and J. Popp, "The Bouguer-Beer-Lambert Law: Shining Light on the Obscure," *ChemPhysChem*, 2020, doi: 10.1002/CPHC.202000464.

[26] "Pulse Oximetry Basic Principles and Interpretation | Iowa Head and Neck Protocols." https://medicine.uiowa.edu/iowaprotocols/pulse-oximetry-basic-principles-and-interpretation.

[27] K. K. Tremper, & J. S. Barker. "Pulse Oximetry".

[28] K. K. Tremper and S. J. Barker, "Pulse Oximetry," *Anesthesiology*, vol. 70, no. 1, pp. 98–108, Jan. 1989, doi: 10.1097/00000542-198901000-00019.

[29] A. C. M. Dassel, R. Graaff, M. Sikkema, A. Meijer, W. G. Zijlstra, and J. G. Aarnoudse, "Reflectance pulse oximetry at the forehead improves by pressure on the probe," *J Clin Monit*, vol. 11, no. 4, pp. 237–244, Jul. 1995, doi: 10.1007/BF01617518.

[30] H. Lee, H. Ko, and J. Lee, "Reflectance pulse oximetry: Practical issues and limitations," *ICT Express*, vol. 2, no. 4, pp. 195–198, Dec. 2016, doi: 10.1016/J.ICTE.2016.10.004.

[31] C. Y. Huang, M. C. Chan, C. Y. Chen, and B. S. Lin, "Novel wearable and wireless ring-type pulse oximeter with multi-detectors," *Sensors (Basel)*, vol. 14, no. 9, pp. 17586–17599, 2014, doi: 10.3390/S140917586.

[32] M. Chan, V. G. Ganti, J. A. Heller, C. A. Abdallah, M. Etemadi, and O. T. Inan, "Enabling Continuous Wearable Reflectance Pulse Oximetry at the Sternum," *Biosensors (Basel)*, vol. 11, no. 12, Dec. 2021, doi: 10.3390/BIOS11120521.

[33] M. Santos *et al.*, "The Use of Wearable Pulse Oximeters in the Prompt Detection of Hypoxemia and During Movement: Diagnostic Accuracy Study," *J Med Internet Res 2022;24(2):e28890 https://www.jmir.org/2022/2/e28890*, vol. 24, no. 2, p. e28890, Feb. 2022, doi: 10.2196/28890.

[34] J. G. Pak and K. H. Park, "Advanced pulse oximetry system for remote monitoring and management," *Journal of Biomedicine and Biotechnology*, vol. 2012, 2012, doi: 10.1155/2012/930582.

[35] C. P. Bonafide *et al.*, "Accuracy of Pulse Oximetry-Based Home Baby Monitors," *JAMA*, vol. 320, no. 7, pp. 717–719, Aug. 2018, doi: 10.1001/JAMA.2018.9018.

[36] G. S. Agashe, J. Coakley, and P. D. Mannheimer, "Forehead pulse oximetry: Headband use helps alleviate false low readings likely related to venous pulsation artifact," *Anesthesiology*, vol. 105, no. 6, pp. 1111–1116, Dec. 2006, doi: 10.1097/00000542-200612000-00010.

[37] G. S. Agashe, J. Coakley, and P. D. Mannheimer, "Forehead Pulse OximetryHeadband Use Helps Alleviate False Low Readings Likely Related to

Venous Pulsation Artifact," *Anesthesiology*, vol. 105, no. 6, pp. 1111–1116, Dec. 2006, doi: 10.1097/00000542-200612000-00010.

[38] W. Chen, S. B. Oetomo, L. Feijs, S. Bouwstra, I. Ayoola, and S. Dols, "Design of an integrated sensor platform for vital sign monitoring of newborn infants at Neonatal Intensive Care Units," *Journal of Healthcare Engineering*, vol. 1, no. 4, pp. 535–554, 2010, doi: 10.1260/2040-2295.1.4.535.

[39] M. I. Dangerfield, K. Ward, L. Davidson, and M. Adamian, "Initial Experience and Usage Patterns With the Owlet Smart Sock Monitor in 47,495 Newborns," *Global Pediatric Health*, vol. 4, 2017, doi: 10.1177/2333794X17742751.

[40] W. Chen, S. B. Oetomo, L. Feijs, S. Bouwstra, I. Ayoola, and S. Dols, "Design of an integrated sensor platform for vital sign monitoring of newborn infants at Neonatal Intensive Care Units," *Journal of Healthcare Engineering*, vol. 1, no. 4, pp. 535–554, 2010, doi: 10.1260/2040-2295.1.4.535.

[41] M. I. Dangerfield, K. Ward, L. Davidson, and M. Adamian, "Initial Experience and Usage Patterns With the Owlet Smart Sock Monitor in 47,495 Newborns," *Global Pediatric Health*, vol. 4, 2017, doi: 10.1177/2333794X17742751.

[42] "(1) (PDF) Initial Experience and Usage Patterns With the Owlet Smart Sock Monitor in 47,495 Newborns." https://www.researchgate.net/publication/321495322_Initial_Experience_and_Usage_Patterns_With_the_Owlet_Smart_Sock_Monitor_in_47495_Newborns.

[43] J. W. Salyer and R.-N. Faarc, "Neonatal and Pediatric Pulse Oximetry Introduction Measurement Principles Accuracy of Oximeters Limitations of Oximetry Motion Artifact, Poor Perfusion, and Oximeter Alarms Processes, Outcomes, and Pulse Oximetry On the Horizon Summary," 2003.

[44] S. S. Panda, M. Panda, R. R. Das, and P. K. Mohanty, "Pulse oximeter probe-induced toe injury in a neonate: A rare avoidable injury," *Journal of Clinical Neonatology*, vol. 3, no. 4, p. 240, 2014, doi: 10.4103/2249-4847.144766.

[45] Y. Ino *et al.*, "Skin burn related to pulse oximetry during photodynamic therapy using talaporfin sodium", doi: 10.1186/s40981-018-0203-0.

[46] "PUL-eez tell me it's safe! A look at the safety of PUL fabric in Cloth – New and Green Baby Co." https://www.newandgreen.com/blogs/news/56943363-pul-eez-tell-me-its-safe-a-look-at-the-safety-of-pul-fabric-in-cloth-diapers

[47] F. Semiconductor Inc, "Crystal-less USB operation on Kinetis MCUs," 2014.

[48] "Pulse Oximeter design solution from Microchip." https://www.rs-online.com/designspark/pulse-oximeter-solution-from-microchip

[49] I. V. Lam, "Analysis of Improved Howland Current Pump Configurations," 2020, Accessed: Apr. 26, 2022. [Online]. Available: www.ti.com

[50] G. Lenis, N. Pilia, A. Loewe, W. H. W. Schulze, and O. Dössel, "Comparison of Baseline Wander Removal Techniques considering the Preservation of ST Changes in the Ischemic ECG: A Simulation Study," *Computational and Mathematical Methods in Medicine*, vol. 2017, 2017, doi: 10.1155/2017/9295029.

[51] "Pulse Transit Time PPG Dataset v1.0.0." https://physionet.org/content/pulse-transit-time-ppg/1.0.0/.

[52] "How Much Does Pulse Oximetry Cost? | Blog | HCP Resources | Medtronic." https://hcpresources.medtronic.com/blog/how-much-does-pulse-oximetry-cost.

Appendix

Appendix A: Images of implemented IR sensor and testing on the finger

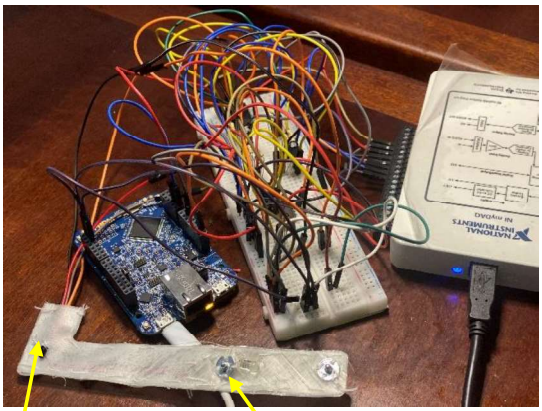

OP999 Photodiode

IR LED

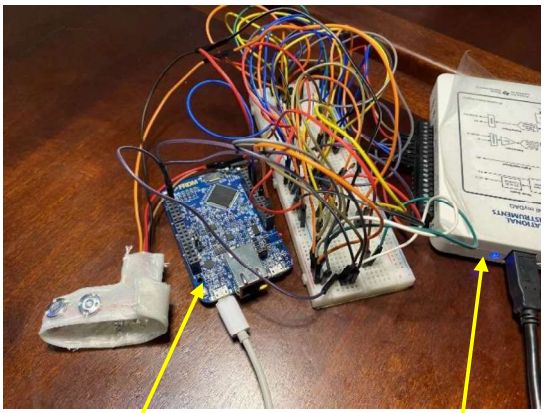

FRDM K64F

NI myDAQ

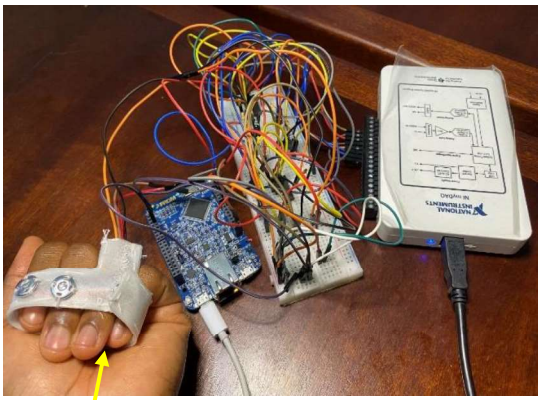

Using my hands instead of the neonate's foot

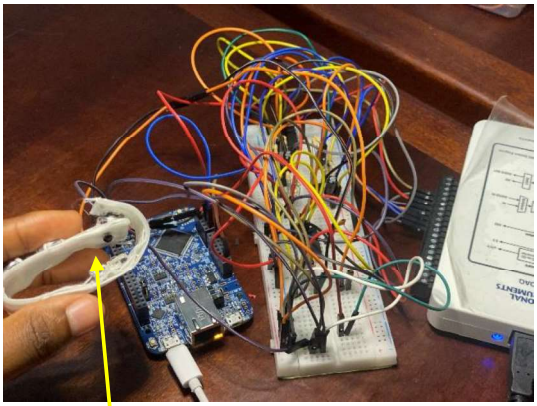

IR LED and photodiode directly opposite each other (transmittance approach)

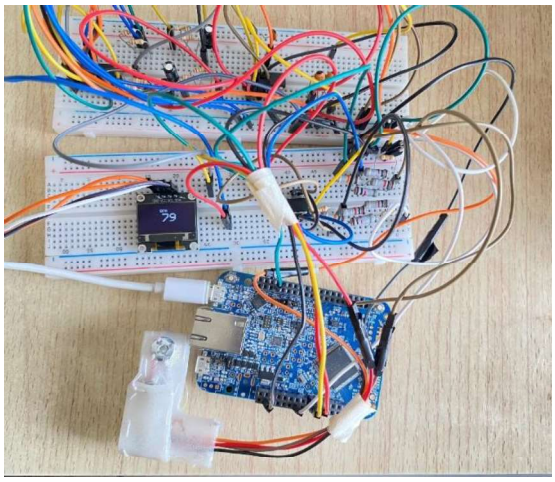

Pulse rate reading (79 bpm) using the built IR Pulse sensor

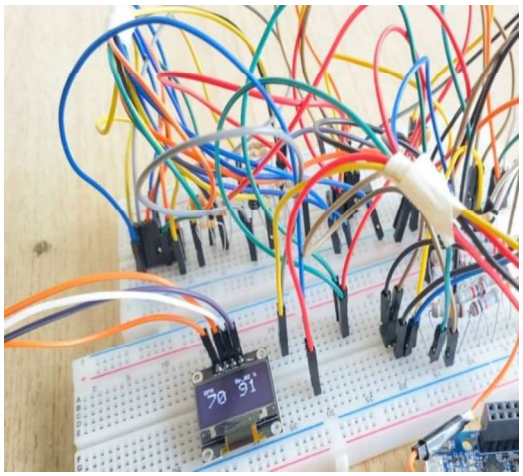

Pulse rate reading (70 bpm) and SpO_2 reading (91%) using obtained PPG data from the Physionet database

Some pulse oximeter readings from the Lk87 pulse oximeter for comparison with the built IR pulse sensor

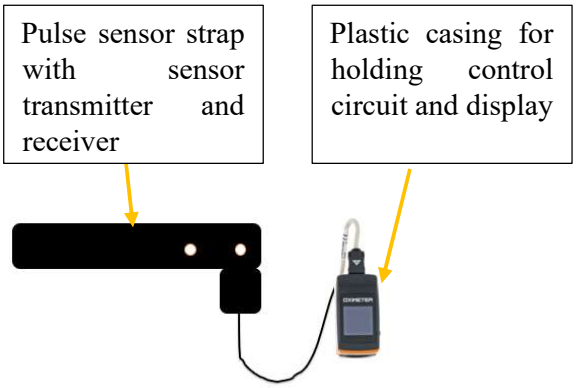

Proposed outlook of the neonatal pulse oximeter

Appendix B: Solidworks design of flap for holding the sensors and casing for holding the electronical control circuit and display

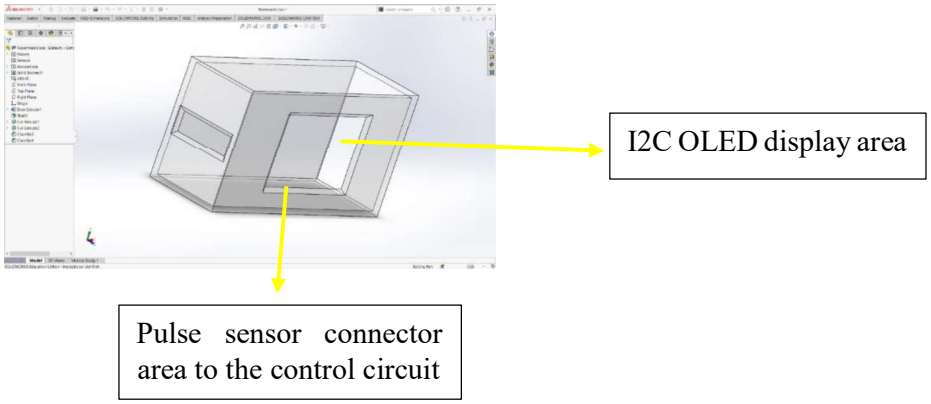

(a) Solid works design for casing for holding electrical control circuit and display

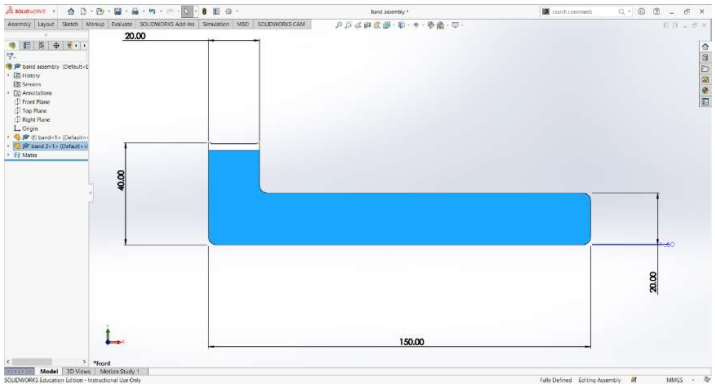

(b) Solid works design for flap for housing red and IR LEDs and light to voltage converter or photodiode

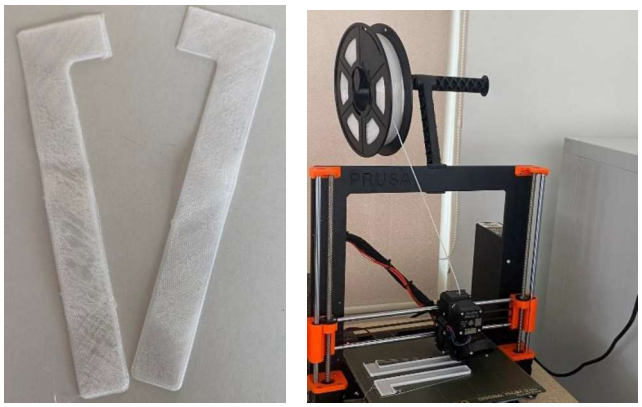

(c) Printed TPU flaps for pulse sensor

Appendix C: Source Code

https://github.com/Tnyatefe/CapstoneCodes